Geochemistry Geophysics Geosystems G3
AN ELECTRONIC JOURNAL OF THE EARTH SCIENCES
Published by AGU and the Geochemical Society

Article
Volume 7, Number 11
21 November 2006
Q11014, doi:10.1029/2006GC001342
ISSN: 1525-2027

A comparison of Siberian meimechites and kimberlites: Implications for the source of high-Mg alkalic magmas and flood basalts

Richard W. Carlson
Department of Terrestrial Magnetism, Carnegie Institution of Washington, 5241 Broad Branch Road, NW, Washington, D. C. 20015, USA (carlson@dtm.ciw.edu)

Gerald Czamanske
750 West Greenwich Place, Palo Alto, California 94303, USA

Valeri Fedorenko
TsNIGRI, Varshavskoye Shosse 129B, Moscow 113545, Russia

Iosif Ilupin
TsNIGRI, Varshavskoye Shosse 129B, Moscow 113545, Russia
Deceased 5 February 2004

[1] Chemical and radiogenic isotope (Sr, Nd, Hf, Os, and Pb) data are presented for a variety of mafic-alkalic rocks from the Maymecha-Kotuy section of the Siberian flood-volcanic province. These data are compared to a similar data set for Siberian kimberlites that were emplaced both before and after the flood-volcanic event in order to examine the spatial-temporal evolution of Paleozoic magma sources in the mantle beneath this site of voluminous magmatic activity. As shown in previous studies, the high-Mg, meimechitic composition rocks extend the range in Sr and Nd isotopic composition seen in the flood basalts in the direction of more "depleted" compositions, i.e., higher $^{143}Nd/^{144}Nd$ and lower $^{87}Sr/^{86}Sr$, overlapping values typically observed in intraplate ocean-island basalts. Sr, Nd, Hf, and Pb isotopic compositions show little correlation with major- and trace-element compositions in the Maymecha-Kotuy rocks. Os isotopic compositions, on the other hand, show rough correlations with a number of major-element characteristics of the magmas. The Os data suggest that the magma sources range from peridotite for the meimechitic magmas to a mixture of peridotite and pyroxenite for the nephelinitic, melilititic, and trachybasaltic compositions. The isotopic overlap of both old and young kimberlites with the Maymecha-Kotuy rocks is consistent with all these magmas being derived from mantle sources that were present beneath Siberia long before, and long after, the flood-volcanic event. The isotopic characteristics of the mantle source of these magmas best match the FOZO component observed in ocean-island basalts, which suggests that this mantle composition may be prevalent in the upper mantle outside of ocean basins. The long-lived presence of this source beneath Siberia makes it unnecessary to appeal to a mechanism, such as a plume, to bring this type of mantle into play only during the flood-volcanic episode.

Components: 12,818 words, 7 figures, 3 tables.

Keywords: flood basalts; kimberlites; magma sources; radiogenic isotopes; Siberia.

Index Terms: 1033 Geochemistry: Intra-plate processes (3615, 8415); 1040 Geochemistry: Radiogenic isotope geochemistry; 1065 Geochemistry: Major and trace element geochemistry.

Received 19 April 2006; **Revised** 18 August 2006; **Accepted** 11 September 2006; **Published** 21 November 2006.

Carlson, R. W., G. Czamanske, V. Fedorenko, and I. Ilupin (2006), A comparison of Siberian meimechites and kimberlites: Implications for the source of high-Mg alkalic magmas and flood basalts, *Geochem. Geophys. Geosyst.*, *7*, Q11014, doi:10.1029/2006GC001342.

1. Introduction

[2] The Siberian continental platform has been the site of extensive magmatic activity during the Phanerozoic, including the eruption of one of the largest continental flood-volcanic provinces on Earth [*Milanovskiy*, 1976; *Fedorenko et al.*, 1996]. As is common in many large igneous provinces, the Siberian lavas include both high- and low-Ti compositional types [e.g., *Lightfoot et al.*, 1990; *Sharma et al.*, 1991; *Fedorenko and Czamanske*, 1997]. Unlike most other provinces, however, the compositional range in Siberian high-Ti lavas is very large and extends well beyond typical basalt, to strongly alkalic-ultramafic magmas and lavas as silicic as trachyrhyodacite [*Arndt et al.*, 1995; *Basu et al.*, 1995; *Fedorenko and Czamanske*, 1997; *Arndt et al.*, 1998]. The most extreme ultramafic compositions are found in the unique meimechitic lavas of the Maymecha-Kotuy region in the northern portion of the flood-volcanic province [*Fedorenko and Czamanske*, 1997; *Arndt et al.*, 1998]. Meimechites are volcanic rocks characterized by high MgO (generally greater than 23 wt%), TiO_2 (~3 wt%) and FeO (~14 wt%) with strong enrichment in incompatible trace elements [*Arndt et al.*, 1995; *Fedorenko and Czamanske*, 1997]. Meimechites approach kimberlite in chemical composition although higher SiO_2 and FeO, and lower CaO distinguish them from typical kimberlites [*Fedorenko et al.*, 2000]. Kimberlites are widely scattered in both space and time throughout Siberia [e.g., *Fedorenko et al.*, 2000], but meimechitic lavas are restricted to the Maymecha-Kotuy area where they form the upper-most units of a nearly 4 km thick sequence of flood lavas [*Fedorenko and Czamanske*, 1997].

[3] The extreme compositional range present in the high-Ti magmas of the Maymecha-Kotuy sequence provides an opportunity to investigate (1) the degree of compositional heterogeneity in the mantle beneath the Siberian flood-volcanic province, (2) the variety of primary magmas that contributed to this event, and (3) the processes that caused the volcanism and determined the compositional characteristics of the eruptive products. Understanding the origin of the low-Mg, and generally low-Ti, basaltic rocks that volumetrically dominate most flood-basalt provinces is compromised by the ambiguity over how much of their composition is determined by crustal-level fractionation processes, including crustal contamination [e.g., *Carlson et al.*, 1981; *Lightfoot et al.*, 1990; *Carlson*, 1991; *Wooden et al.*, 1993; *Mahoney and Coffin*, 1997]. In contrast, in the Siberian flood-volcanic province, many of the high-Ti magma types have high MgO and Ni contents consistent with equilibrium between the erupted melt and mantle peridotite [*Arndt et al.*, 1998]. These characteristics imply rapid transit of the magma through the crust with limited opportunity for either fractionation or contamination. Furthermore, the very high incompatible-element concentrations in the mafic to ultramafic alkalic magmas make the Sr-Nd-Hf-Pb isotopic systems in these magmas relatively insensitive to crustal additions, improving the ability to document isotopic variability in the mantle source. In addition, the compositional similarity of meimechite and kimberlite allows an opportunity to compare the composition of the magma sources during the flood-volcanic event with the mantle that was present both long before, and well after, it occurred. Thus comparison of Siberian kimberlite and meimechite compositional characteristics potentially can address the issue of whether a compositionally distinct mantle source had to be delivered beneath this area to produce the flood lavas, for example by a deep mantle plume, or, alternatively, whether the magmatism simply sampled the mantle beneath Siberia.

[4] To investigate this question, we report new major- and trace-element and Sr, Nd, Hf, Os and Pb isotopic data for a suite of samples that includes a variety of mafic-alkalic compositions from the Maymecha-Kotuy stratigraphic section of the Siberian flood-volcanic province. Also reported are Sr, Nd, Hf and Pb isotopic data for kimberlites from within, and to the east of, the flood-volcanic

province, which were emplaced from ~156 to 475 Ma, a span that encompasses the period of flood volcanism (~251 Ma [*Kamo et al.*, 2003]).

2. Sample Descriptions and Regional Context

[5] The magmatic stratigraphy of the Maymecha-Kotuy region was described in detail in *Fedorenko and Czamanske* [1997] from which the following brief summary is extracted. The Maymecha-Kotuy area is located in the northern portion of the Siberian Platform approximately 500 km east-northeast of Noril'sk and 300–500 km west of the Anabar Shield (Figure 1). Permo-Triassic igneous rocks in this area cover roughly 70,000 km^2 and present a nearly 4 km-thick stratigraphic sequence of lavas and shallow intrusive rocks. The lower 1500 m of the stratigraphic sequence in the Maymecha-Kotuy region consists primarily of low-Ti basalts that can be correlated with similar basalts in the Noril'sk locality to the southwest. The major fraction of the stratigraphic sequence at Maymecha-Kotuy consists of high-Ti compositions ranging from primitive, high-MgO, lavas such as the meimechites to more evolved rocks extending to trachyrhyodacites. The more primitive compositions in this sequence include mela-nephelinite, limburgite, picrite, and meimechite. The sequence also contains a variety of intrusive rocks including various ultramafic-alkalic compositions in the subvolcanic Guli intrusion, which itself contains two carbonatite intrusions. The samples studied here concentrate primarily on the high-MgO end of the compositional spectrum available in the Maymecha-Kotuy region.

[6] U-Pb dating of various mineral phases extracted from flows and intrusions from the Maymecha-Kotuy area, including the carbonatites in the Guli intrusion, provide ages ranging from 251.7 ± 0.4 Ma in the lowermost units to 251.1 ± 0.3 Ma in the upper portions of the stratigraphic section [*Kamo et al.*, 2003]. This limited age range suggests that the whole igneous stratigraphy in the Maymecha-Kotuy area was deposited in less than 1 Ma and is contemporaneous with other sections of the Siberian flood-volcanic rocks, such as those studied in the Noril'sk and Putorana regions [*Kamo et al.*, 1996].

[7] Scattered around the Anabar Shield are a number of kimberlite fields whose ages range from Ordovician to Cretaceous [*Davis et al.*, 1980], although age information is not available for all the kimberlite intrusions in this area (Figure 1). General petrographic [*Bobrievich et al.*, 1964] and geochemical data [*Ilupin*, 1981; *Agashev et al.*, 2000; *Golubeva and Tsepin*, 2004] for these kimberlites mostly have been published in the Russian literature.

[8] Samples selected for this study cover a range of compositions within the mafic-alkalic suite of Maymecha-Kotuy and include both extrusive and intrusive units along with intrusive rocks from both the Guli massif (sample numbers beginning with 4) and the Kresty massif (sample numbers beginning with 5). Four compositional groups are present in the Maymecha-Kotuy sample suite. Samples 2FG-22 and G-3/100 are meimechites from the Upper Maymechinsky subsuite [*Fedorenko and Czamanske*, 1997]. 2FG-22 is the quenched crust of a meimechite flow while G-3/100, which samples one of the glass-rich, olivine-poor, regions in the 500 m deep G-3 drill core, is interpreted to be a residual liquid left after in-situ crystallization of a meimechite flow [*Fedorenko and Czamanske*, 1997]. Sample 2FG-99 is a meimechite-related limburgite-picrite from the Middle Delkansky subsuite [*Fedorenko and Czamanske*, 1997]. The mela-nephelinite compositional group is represented by lava sample 1FG-213 and dike sample 1FG-239, both of which are from the lower Delkansky subsuite. Rocks from the melilite-related compositional group (the Arydzhangsky Suite) include limburgite 3FG-13, olivine mela-nephelinite 3FG19, and melilitite 3FG-20. From the more evolved compositions present in the section, sample 2FG-73 from a trachydolerite dike that cuts the meimechitic lavas was analyzed. From the Guli massif we analyzed dunite 4FG-32, peridotitic-ankaratrite 4FG-50, and ijolite-melteigites 4FG-17 and 4FG-24. As reported by *Fedorenko and Czamanske* [1997], an ankaratrite is a melanocratic nepheline basalt with abundant clinopyroxene and olivine, plus or minus melilite. The final samples come from the Kresty massif, an intrusion also dominated by olivine-rich rocks, but distinguished from the Guli massif by an abundance of perovskite and monticellite. Sample 5FG-34 is a perovskite-olivinite containing 25–30% perovskite (V. A. Fedorenko and G. K. Czamanske, unpublished data, 2000). Sample 5FG-67 is composed of olivine, monticellite, and ~8% perovskite.

[9] Kimberlites, all from the collection of I. P. Lupin, were selected for study specifically to include a wide age range in order to investigate possible temporal variation/evolution in magma

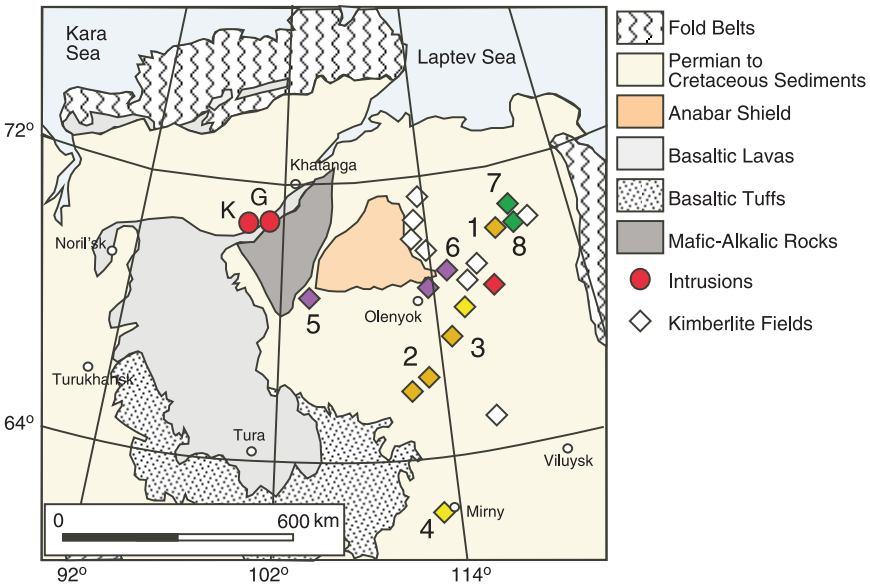

Figure 1. Location of the Maymecha-Kotuy region of mafic-alkalic volcanism (dark gray) in comparison to other regions of the Siberian flood-volcanic province dominated either by basaltic lavas (light gray) or by basaltic tuffs (stippled pattern). Diamonds show the location of Yakutian kimberlite fields color-coded according to age as follows: red, Ordovician; yellow, Ordovician and Devonian; brown, Devonian; purple, Late Carboniferous to Triassic; green, Jurassic and Cretaceous; and white, age not determined. Labeled kimberlite fields pertinent to this report include (1) Merchimden, (2) Daldyn, (3) Upper Muna, (4) Malaya Botuobiya, (5) Kharamay, (6) Luchakan, (7) Kuoyka, and (8) Upper Molodo. Large red circles show the location of the Guli and Kresty mafic-alkalic intrusions. Archean rocks of the Anabar Shield are shown in light brown, Late Proterozoic to Cretaceous sediments surrounding the craton are shown in light yellow, and fold belts surrounding the craton are shown by the wavy pattern.

source composition (Table 3). Whereas some of the Siberian kimberlites include psammitic, sand-size xenoliths, only xenolith-free rocks and rocks with rather large xenoliths were chosen for analysis. All weathered crusts and traces of contamination were removed, and each sample was crushed to <5–8 mm. At this stage all xenolith fragments and large (>2–3 mm) veinlets and pockets of secondary minerals (veinlets of calcite were most prevalent) were removed by hand picking. Large phenocrysts of olivine (and their pseudomorphs), mica, ilmenite and garnet (pyrope) were considered part of the sample. Not less than 100 g of material was crushed to <0.5 mm in a steel mortar and pulverized in a porcelain mortar.

[10] Most of the samples analyzed predate the flood-volcanic episode. The oldest sample (Pd-2/25) is from the Podsnezhnaya pipe in the Merchimden field (Figure 1), and has an age of 475 Ma, as determined by fission track dating of zircon megacrysts [*Komarov and Ilupin*, 1990]. The sample is quite altered as indicated by the high abundance of carbonate veining and the lack of fresh olivine. Of the four Devonian kimberlites analyzed here, sample ZK-18 from the Zarnitza pipe in the Daldyn field also suffers both carbonate contamination and substantial alteration of the olivine present. The sample also contains a moderate amount of ilmenite that likely is xenocrystal. The other Devonian samples, US217-170 from the Udachnaya-E pipe in the Daldyn cluster, NV4/4 from the Novinka pipe of the Upper Muna field, and R-19-K from the Mir pipe of the Malaya Botuobiya field are not affected by carbonate contamination. Olivine phenocrysts, abundant in all three samples, are altered in NV4/4 and R-19-K, but relatively fresh in US217-170. Of these three samples, only R-19-K contains a moderate amount of ilmenite; it is the only one of these three samples with a precise U-Pb date measured on zircon megacrysts [*Davis et al.*, 1980].

[11] Sample ES12/42 is the only kimberlite sample similar in age to the Maymecha-Kotuy igneous rocks. This sample is from the Podsnezhnaya pipe in the Kharamay field, which is the most westerly of the Yakutian kimberlite fields; it has a suggested age of 250 Ma based on a wide range of fission

track ages (236–290 Ma) determined for the Kharamay pipes by *Komarov and Ilupin* [1990].

[12] Three kimberlites analyzed in this study postdate the flood-volcanic activity. These include: P-14088 from the Pozdnyaya pipe in the Luchakan field in the central part of the province; Ol-R-52 from the Ruslovaya pipe in the Kuoyka field to the northeast; and Me-5211 from the Mery pipe in the Upper Molodo cluster, also in the northeast. P-14088 is not carbonate veined, but contains no fresh olivine and moderate amounts of ilmenite. The age for this sample was determined by U-Pb zircon analysis [*Davis et al.*, 1980]. Sample Ol-R-52 contains abundant fresh olivine, but no ilmenite; the age was determined by fission track analysis of zircon megacrysts [*Komarov and Ilupin*, 1990]. Me-5211 is quite highly altered with abundant carbonate veining, no fresh olivine, and abundant ilmenite. The age for this sample is assumed, based on the observation that all other pipes of the Upper Molodo cluster have U-Pb zircon ages of 156–159 Ma [*Davis et al.*, 1980] and fission track ages of 150–171 Ma [*Komarov and Ilupin*, 1990].

3. Analytical Procedures

[13] Major- and trace-element compositions were determined in the Denver laboratories of the United States Geological Survey using the methods described by *Baedecker* [1987]. Major elements were determined by X-ray fluorescence. The rare earth element (REE) data and most of the minor-element data of Table 1 were determined by instrumental neutron activation analysis (INAA). Data for Ba, Cr, Ni, Rb, Sr, Zn, and Zr were determined by energy-dispersive, X-ray fluorescence for all samples except those whose designations include 4FG and 5FG; for these samples, data for these elements was obtained by INAA. All of the trace-element data in Tables 2 and 3 were obtained at the Department of Terrestrial Magnetism (DTM) by isotope dilution (ID).

[14] Isotopic analyses were performed at DTM. Approximately 50–100 mg of sample powder was dissolved for Sr, Nd, Hf and Pb isotopic determinations. Before dissolution, the samples were spiked with enriched tracers of ^{87}Rb, ^{84}Sr, ^{150}Nd, ^{149}Sm, ^{176}Lu, ^{178}Hf, ^{205}Pb and ^{235}U. All samples were dissolved in sealed 15 ml Savillex beakers, in approximately 3ml concentrated HF plus 1 ml concentrated HNO_3 and left on a 90°C hotplate for 2–4 days. Samples were then evaporated to dryness and treated twice with 1 ml of concentrated HNO_3 (drying in between treatments), followed by addition of ~2 ml of 0.5N HBr. The samples were dried again and taken up in 3 ml of 0.5N HBr. Samples in HBr were loaded onto 0.04 ml columns containing pre-cleaned AG1-X8 anion-exchange resin. All matrix elements were eluted in 0.5N HBr followed by elution of Pb in 0.5N HNO_3. The Pb split was dried, redissolved in 0.5N HBr and passed through the Pb column a second time.

[15] The solution containing the matrix elements was dried, and then oxidized by adding 1 ml of water followed by 1 ml of concentrated HNO_3. The solution was dried, redissolved in 4N HCl and dried again before the addition of 5ml 1N HCl-0.1N HF. This solution was loaded on a 0.6 × 20 cm column of AG50W-X8 cation-exchange resin. Hf was collected from the loading solution and an additional 5 ml of 1N HCl-0.1N HF. The eluant was then changed to 2.5N HCl. Rb and U were collected between 12–22 ml and Sr between 30–44 ml. Switching to 4N HCl, the REE were eluted as a group in 28 ml.

[16] Hf was further purified in a 1 ml column of LN-spec resin loading in 3N HCl, followed by washes in 3N HCl, 6N HCl, H_2O, and a solution of 0.09N citric acid-0.45N HNO_3-1wt%H_2O_2 to elute Ti. The column was then washed with 6N HCl-0.06N HF, which removes some Zr, and then 6N HCl-0.4N HF, which eluted the Hf.

[17] Sm, Nd and a heavy REE split were separated from the REE fraction using a 0.2 × 20 cm column filled with AG50-X8 resin in NH^{3+} form. Samples were loaded in 0.04 ml of 0.1N HCl and then eluted in α-hydroxyisobutyric acid. Lu was separated from the heavy REE split using a 4 mm ID by 70 mm long column filled with LN-spec resin. The heavy REE cut was dissolved and loaded in 0.05 ml of 0.25N HCl then washed with 33 ml of 2.5N HCl. Lu was then collected in 6 ml of 6N HCl. U was separated from Rb using a 0.25 ml column of TRU resin. The sample was loaded in 1.5 ml of 2N HNO_3 with Rb collected from both the loading volume and a subsequent wash with 4 ml of 2N HNO_3. U was then eluted with 4 ml of 0.1N HCl-0.3N HF.

[18] For Re-Os determinations, approximately 2 g of sample powder was weighed into pyrex carius tubes along with enriched tracer solutions of ^{185}Re and ^{190}Os. The dissolution acid consisted of 6 ml concentrated HNO_3 and 3 ml concentrated HCl, all of which was frozen into the bottom of the carius

Table 1. Major- and Trace-Element Compositions of Samples From the Maymecha-Kotuy Region[a]

Sample Type	2FG-22 Meim	G-3/100 Meim	2FG-99 Lim-Pic	1FG-239 Mneph	1FG-213 Mneph	3FG-13 Limb	3FG-19 Mel	3FG-20 Mel	2FG-73 Tbasalt	4FG-17 Ijolite	4FG-24 Ijolite	4FG-32 Dunite	4FG-50 P-ank	5FG-34 Per-ol	5FG-67 Ol-mt
SiO_2	42.42	40.38	45.14	43.21	44.74	44.30	41.27	40.84	44.46	36.82	40.49	39.69	40.67	18.87	26.93
TiO_2	1.99	4.89	4.56	2.99	3.53	3.63	3.90	3.84	3.05	6.80	2.75	0.17	1.53	14.22	9.18
Al_2O_3	2.36	5.27	7.05	4.16	7.03	9.64	6.10	5.87	9.09	3.91	2.42	0.16	1.37	1.24	1.38
FeO_T	12.14	16.07	14.37	12.01	12.45	12.67	15.06	14.93	13.37	16.41	17.07	13.63	12.06	35.43	19.48
MnO	0.18	0.22	0.26	0.17	0.18	0.19	0.21	0.21	0.20	0.21	0.26	0.22	0.18	0.28	0.25
MgO	36.42	15.83	13.11	26.70	13.11	12.86	15.11	15.27	13.72	10.93	24.79	45.33	38.94	22.58	16.33
CaO	3.82	14.45	12.16	7.94	15.71	12.54	13.86	14.02	12.27	21.65	10.42	0.58	4.18	7.11	25.79
Na_2O	0.12	0.34	1.42	1.62	1.60	2.64	2.21	3.19	1.99	1.18	0.69	0.11	0.66	0.18	0.39
K_2O	0.08	1.87	1.34	0.85	1.19	0.99	1.69	1.18	1.41	0.81	0.90	0.02	0.15	0.05	0.14
P_2O_5	0.47	0.67	0.59	0.36	0.46	0.55	0.59	0.64	0.44	1.27	0.22	0.08	0.24	0.06	0.12
LOI	11.8	3.45	3.47	0.81	2.18	5.30	5.79	3.73	1.30	0.29	0.14	7.52	0.45	5.98	
Rb	8.00	55.0	30.0	17.8	72.0	89.0	120	100	32.0	20.5	18.1	5.38	3.92	3.62	4.24
Ba	130	510	355	320	620	1870	526	2230	490	501	289	9.16	134	77.3	48.8
Th	2.16	6.02	6.23	8.52	8.20	13.6	14.4	14.5	3.91	18.3	0.70	0.11	0.21	175	204
U	1.54	1.52	1.11	1.49	1.29	1.06	3.50	3.51	1.00	4.44	0.43	0.09	0.08	6.95	8.63
Ta	1.96	5.75	6.09	4.60	6.04	11.6	12.8	12.7	3.10	13.5	1.32	0.04	1.36	58.6	61.3
Ce	55	148	138	183	160	297	306	308	89	371	42	1.02	43	2230	3020
Sr	320	850	750	1087	1200	2510	1450	3730	800	1250	588	76.4	262	654	1110
Nd	28.7	70.9	65.4	70.5	66.4	111	111	111	39.5	158	25.1	0.42	22.5	1010	1260
Hf	3.42	8.52	8.34	7.56	7.47	8.82	7.92	8.09	5.17	8.94	3.67	0.06	2.22	3.06	3.96
Zr	152	395	340	337	310	422	361	391	225	357	192	18.8	90.4	278	398
Sm	5.5	13.7	12.9	10.7	11.2	15.2	14.9	15.0	8.2	27.5	4.9	0.1	4.1	121	142
Eu	1.45	3.76	3.40	2.70	2.84	3.79	3.56	3.61	2.31	7.51	1.32	0.03	1.09	22.3	30.1
Gd	3.87	9.57		7.31		11.1	9.94	11.0		19.3	3.24	0.09	2.72	46.9	65.2
Tb	0.41	1.17	1.08	0.94	0.93	1.07	1.02	1.09	0.77	2.18	0.43	0.01	0.34	4.15	5.79
Yb	0.55	1.49	1.66	1.15	1.43	1.55	1.47	1.48	1.35	1.87	0.62	0.03	0.39	0.67	2.58
Lu	0.07	0.18	0.22	0.12	0.17	0.19	0.20	0.19	0.18	0.22	0.10	0.00	0.06	0.10	0.27
Sc	12.6	29.7	32.3	21.0	43.8	20.4	25.9	26.3	35.8	59.9	36.6	4.48	13.4	23.1	14.3
V	140	360	330	271	300				350						
Cr	1900	940	900	1019	640	458	586	598	550	221	2360	2420	2430	572	222
Co	112	90.3	74.6	95.0	67.1	60.7	75.0	78.4	75.7	64.3	136	142	128	153	104
Ni	1500	430	365	1286	255	328	397	426	345	201	1050	2340	2210	1180	653
Zn	86	116	70	102	83	108	129	123	93	139	126	81	86	154	175

[a] Oxides are listed in weight percent; trace elements are in ppm. Major-element concentrations are normalized to total 100%, not including loss on ignition (LOI). Rock type abbreviations are as follows: Mneph, melanephelinite; Meim, meimechite; Tbasalt, trachybasalt; Lim-Pic, limburgite-picrite; Mel, melilitite; Perid, peridotite; P-ank, peridotite-ankaratrite; Per-ol, perovskite-olivinite; ol-mt, olivine-monticellite.

Table 2. Radiogenic-Isotope Compositions of Maymecha-Kotuy Samples[a]

Sample	2FG-22	G-3/100	2FG-99	1FG-239	1FG-213	3FG-13	3FG-19	3FG-20	2FG-73	4FG-17	4FG-24	4FG-32	4FG-50	5FG-34	5FG-67
Rb (ppm)	5.28	58.1	27.5	17.5	72.4	50.5		37.8	25.0	12.2	16.1			1.50	3.28
Sr (ppm)	334	869	759	1071	1169	2477	1513	3539	780	1212	342		331	565	1040
$^{87}Rb/^{86}Sr$	0.0457	0.1957	0.1061	0.0473	0.1814	0.0597		0.0309	0.0939	0.029	0.136			0.0078	0.0092
$^{87}Sr/^{86}Sr$ (m)	0.703612	0.703913	0.704414	0.703425	0.705112	0.703978	0.704471	0.703963	0.704240	0.703234	0.703658		0.703250	0.703714	0.703829
$^{87}Sr/^{86}Sr$ (i)	0.703449	0.703214	0.704035	0.703256	0.704464	0.703765		0.703853	0.703905	0.703130	0.703172			0.703686	0.703796
Sm (ppm)	4.91	13.13	12.31	10.43	10.73	14.21	13.90	13.98	7.96	27.84	4.16		3.82	110	149
Nd (ppm)	27.58	73.86	70.82	70.27	69.45	106.7	106.5	107.3	44.56	173.5	21.60		21.57	1006	1296
$^{147}Sm/^{144}Nd$	0.1077	0.1075	0.1047	0.0897	0.0934	0.0805	0.0789	0.0788	0.1080	0.0970	0.1165		0.1069	0.0661	0.0693
$^{143}Nd/^{144}Nd$ (m)	0.512800	0.512789	0.512657	0.512828	0.512567	0.512641	0.512553	0.512581	0.512708	0.512796	0.512763		0.512751	0.512605	0.512583
$^{143}Nd/^{144}Nd$ (i)	0.512623	0.512612	0.512485	0.512681	0.512414	0.512509	0.512423	0.512452	0.512531	0.512637	0.512572		0.512575	0.512496	0.512469
$\varepsilon_{Nd}(i)$	6.0	5.8	3.4	7.2	2.0	3.8	2.2	2.7	4.3	6.3	5.0		5.1	3.6	3.1
T_{dm} (Ga)	0.50	0.52	0.69	0.40	0.74	0.58	0.68	0.64	0.64	0.46	0.61		0.57	0.56	0.60
Lu (ppm)	0.0692	0.189	0.213	0.150	0.185	0.189	0.180	0.182	0.181	0.218	0.0801		0.0561	0.105	0.294
Hf (ppm)	3.614	9.358	8.829	7.827	7.766	9.200	8.327	8.446	5.428	9.694	3.419		2.328	3.417	4.764
$^{176}Lu/^{177}Hf$	0.00271	0.00286	0.00352	0.00271	0.00338	0.00291	0.00306	0.00305	0.00473	0.00318	0.00332		0.00340	0.00646	0.00873
$^{176}Hf/^{177}Hf$ (m)	0.282929	0.282866	0.282741	0.282923	0.282676	0.282729	0.282684	0.282697	0.282805	0.282880	0.282839		0.282857	0.282713	0.282735
Error	0.00001	0.000006	0.000006	0.000006	0.000005	0.000006	0.000006	0.000005	0.000005	0.000006	0.000007		0.000008	0.000011	0.000006
$^{176}Hf/^{177}Hf$ (i)	0.282916	0.282852	0.282724	0.282910	0.282660	0.282715	0.282669	0.282682	0.282782	0.282865	0.282823		0.282840	0.282682	0.282693
$\varepsilon_{Hf}(i)$	10.8	8.5	4.0	10.6	1.7	3.7	2.1	2.5	6.1	9.0	7.5		8.1	2.5	2.9
T_{dm} (Ga)	0.49	0.57	0.74	0.50	0.82	0.75	0.81	0.80	0.65	0.56	0.61		0.59	0.78	0.75
Re (ppb)	0.029	0.102	0.072	0.115	0.284	0.044	0.026	0.036	0.629	0.392	0.235	0.411	0.412	0.442	0.309
Os (ppb)	11.70	0.778	0.337	0.851	0.213	0.241	0.281	0.216	0.220	0.150	1.749	0.943	1.103	2.383	0.425
$^{187}Re/^{188}Os$	0.012	0.846	1.028	0.654	6.482	0.875	0.454	0.807	13.91	12.648	0.648	2.100	1.804	0.893	3.516
$^{187}Os/^{188}Os$ (m)	0.12327	0.12888	0.14619	0.14409	0.17776	0.14081	0.14500	0.14446	0.20695	0.17569	0.12740	0.12817	0.13067	0.12649	0.14240
Error	0.00024	0.00067	0.00027	0.00165	0.00101	0.00026	0.00025	0.00017	0.00012	0.00033	0.00019	0.00022	0.00038	0.00026	0.00040
$^{187}Os/^{188}Os$ (i)	0.12322	0.12534	0.14188	0.14135	0.15060	0.13714	0.14310	0.14108	0.14865	0.12269	0.12469	0.11937	0.12311	0.12275	0.12766
γ_{Os} (i)	−2.92	−1.25	11.79	11.37	18.65	8.05	12.75	11.16	17.12	−3.33	−1.76	−5.95	−3.00	−3.29	0.59
T_{MA}(Ga)	0.77	0.03	1.71	3.88	0.48	1.59	26.43	2.43	0.35	0.23	−0.35	−0.02	0.09	−0.28	0.27
U (ppm)	1.48		0.99	1.81	1.30			2.74	0.97	4.56			0.053	5.33	
Pb (ppm)	1.65	4.32	4.33	4.16	5.73	9.13	8.40	8.65	3.78	2.01	1.76		0.47	3.16	5.01
$^{238}U/^{204}Pb$	59.6	27.3	14.4	28.3	14.6	7.31	27.3	20.8	16.2	174	15.5		7.18	408	245
$^{206}Pb/^{204}Pb$ (m)	20.685	19.130	18.003	19.273	18.598	18.537	19.384	19.370	18.433	24.978	18.470		18.344	38.098	26.564
$^{207}Pb/^{204}Pb$ (m)	15.802	15.530	15.440	15.537	15.528	15.532	15.576	15.569	15.493	15.864	15.523		15.473	16.536	15.944
$^{208}Pb/^{204}Pb$ (m)	39.78	39.25	38.69	39.45	39.38	39.55	39.81	39.75	38.50	47.25	38.42		38.37	224.27	120.88
$^{206}Pb/^{204}Pb$ (i)	18.32	18.05	17.43	18.15	18.02	18.25	18.30	18.55	17.79	18.06	17.85		18.06	21.89	16.83
$^{207}Pb/^{204}Pb$ (i)	15.68	15.47	15.41	15.48	15.50	15.52	15.52	15.53	15.49	15.51	15.49		15.46	15.71	15.44
$^{208}Pb/^{204}Pb$ (i)	38.65	38.09	37.51	37.74	38.18	38.31	38.36	38.33	37.65	38.22	38.10		38.00	51.14	46.02

[a] Initial isotopic compositions are calculated for an age of 251 Ma. Pb isotopic compositions are age corrected on the basis of U and Pb concentrations by ID, when available, or with the U and Th concentrations measured by INAA reported in Table 1.

Table 3. Major-Element and Radiogenic-Isotope Compositions of Kimberlites From Siberia[a]

Sample Pipe	Me-5211 Mery	OL-R-52 Ruslovaya	P-14088 Pozdnyaya	ES-12/42 Podsnez.	R-19-k Mir	Nv-4/4 Novinka	US-217-170 Udachnaya-E	ZK-18 Zarnitza	Pd-2/25 Podsnez.
Age (Ma)	156	158	217	250	361	365	365	376	475
SiO_2	28.16	42.23	37.18	33.31	40.75	35.27	36.86	32.66	33.92
TiO_2	5.25	0.10	4.11	1.96	1.97	1.90	1.56	2.79	0.86
Al_2O_3	2.92	1.14	4.42	3.43	2.66	2.23	2.68	3.18	1.80
Fe_2O_{3T}	13.27	8.68	12.77	11.00	9.52	10.98	11.11	9.78	12.65
MnO	0.21	0.12	0.16	0.21	0.12	0.19	0.17	0.13	0.20
MgO	27.01	44.73	26.20	31.65	37.65	36.79	38.31	28.40	36.35
CaO	20.91	2.51	11.20	15.29	6.71	10.24	7.77	21.84	11.73
Na_2O	0.33	0.06	0.26	0.14	0.05	0.15	0.10	0.05	0.13
K_2O	1.24	0.15	2.80	1.56	0.25	1.41	0.95	0.63	0.54
P_2O_5	0.69	0.27	0.91	1.44	0.31	0.85	0.48	0.55	1.82
LOI	22.93	10.67	8.91	17.17	18.26	17.74	16.09	21.20	19.45
CO_2	18.90	2.36	2.35	8.57	6.70	6.27	4.33	13.06	11.60
Rb (ppm)	65.1	5.84	91.5	2.81	6.88	93.5	76.5	27.4	22.7
Sr (ppm)	1143	311	465	1570	208	585	358	686	870
$^{87}Rb/^{86}Sr$	0.1668	0.0542	0.5697	0.0052	0.0959	0.4626	0.6188	0.1158	0.0756
$^{87}Sr/^{86}Sr$ (m)	0.705637	0.705309	0.705639	0.704203	0.707449	0.706220	0.707279	0.707085	0.704001
$^{87}Sr/^{86}Sr$ (i)	0.705267	0.705187	0.703877	0.704185	0.706956	0.703816	0.704064	0.706465	0.703490
Sm (ppm)	7.81	3.94	13.12	12.48	3.84	8.76	5.66	6.53	16.07
Nd (ppm)	56.67	28.23	91.16	83.15	25.86	65.33	42.06	49.77	123.2
$^{147}Sm/^{144}Nd$	0.0833	0.0845	0.087	0.0907	0.0898	0.0810	0.0813	0.0794	0.0789
$^{143}Nd/^{144}Nd$ (m)	0.512774	0.512737	0.512700	0.512644	0.512626	0.512565	0.512578	0.512547	0.512561
$^{143}Nd/^{144}Nd$ (i)	0.512689	0.512650	0.512576	0.512496	0.512414	0.512371	0.512384	0.512352	0.512316
ε_{Nd} (i)	5.0	4.2	4.3	3.5	4.7	4.0	4.2	3.9	5.7
T_{dm} (Ga)	0.44	0.49	0.54	0.63	0.65	0.67	0.66	0.68	0.67
Lu (ppm)	0.0752	0.0413	0.140	0.0966	0.0776	0.0596	0.0507	0.0694	0.125
Hf (ppm)	3.204	0.4250	5.801	5.176	1.777	2.960	2.205	2.914	11.19
$^{176}Lu/^{177}Hf$	0.00332	0.01372	0.00342	0.00264	0.00617	0.00285	0.00325	0.00337	0.00158
$^{176}Hf/^{177}Hf$ (m)	0.282851		0.282870	0.282904	0.282812	0.282691	0.282707	0.282684	0.282653
Error	0.000007		0.000012	0.000008	0.000011	0.000011	0.000010	0.000010	0.000005
$^{176}Hf/^{177}Hf$ (I)	0.282841		0.282856	0.282891	0.282769	0.282671	0.282684	0.282659	0.282638
ε_{Hf}(I)	6.0		7.9	9.9	8.1	4.7	5.2	4.6	6.1
T_{dm} (Ga)	0.59		0.57	0.52	0.65	0.80	0.78	0.81	0.85
U(ppm)		1.49	3.18		0.64	3.41	1.95	3.16	3.43
Pb(ppm)	5.77	3.14	3.55	9.72	2.91	3.96	4.03	2.66	8.37
$^{238}U/^{204}Pb$		30.85	61.49		14.60	59.41	32.80	84.61	28.54
$^{206}Pb/^{204}Pb$	19.599	19.413	21.003	18.770	19.996	21.231	20.698	22.501	21.830
$^{207}Pb/^{204}Pb$	15.595	15.582	15.656	15.497	15.574	15.662	15.632	15.763	15.725
$^{208}Pb/^{204}Pb$	39.86	39.35	41.80	38.73	39.89	41.87	41.05	43.34	42.01
$^{206}Pb/^{204}Pb$ (i)		18.65	18.89		19.16	17.77	18.79	17.42	19.65
$^{207}Pb/^{204}Pb$ (i)		15.54	15.55		15.53	15.48	15.53	15.49	15.60

[a]Major-element compositions are normalized to 100%, excluding LOI. Initial isotopic compositions are calculated at the eruption age for each kimberlite as given at the top of the table.

tube by immersing the tube in a solid CO_2 - methanol slurry. The carius tubes were welded shut and placed into an oven at 240°C overnight. Samples were removed from the oven, allowed to cool, then placed in an ultrasonic bath for at least one hour before being returned to the 240°C oven overnight. After cooling, the carius tubes were again frozen, the top of the tube broken off, and the sample solution transferred to a 50 ml test tube. Os was separated by three extraction steps into a total of 9 ml of CCl_4 and then back extracted into 4 ml of concentrated HBr. After drying, the Os sample was dissolved in 30 μl of a chromic-sulfuric acid mixture and purified using the microdistillation technique described by *Roy-Barman and Allègre* [1994]. Re was separated from the HCl-HNO_3 solution remaining after Os extraction by first drying and then redissolving in 10ml of 1N HCl. The sample was placed on a 6 mm ID by 4 cm long column containing precleaned AG1-X8 anion exchange resin. The sample was washed with 10 ml of 1N HCl, 2 ml of 0.8 N HNO_3, and 2 ml of 4N HNO_3 before eluting the Re in 10 ml of 4N HNO_3. The Re sample was then dried and redissolved in 1 ml of 0.1N HCl and placed onto a 3 mm ID by 25 mm long column containing precleaned AG1-X8 anion exchange resin. The sample was washed with 8 ml of 0.1N HNO_3 and the Re then eluted in 5 ml of 8N HNO_3.

[19] Isotopic compositions of Rb, Sm, Lu and U for isotope-dilution concentration determinations were measured on the DTM VG-P54 multiple-collector ICP-MS. Sm measurements were done statically using 9 faraday cups, monitoring Nd and Gd as potential interferences and correcting internally for mass fractionation to $^{147}Sm/^{152}Sm$ = 0.56081. For Rb, Lu, and U, instrument fractionation was determined by normalizing to bracketing standard runs. Rb and Lu were measured statically in faraday cups whereas the majority of U measurements were obtained on the Daly electron multiplier. Concentration precisions from these measurements are estimated at: Rb 1%; Sm 0.2%; Lu 1%; U 5%.

[20] Hf isotopic compositions were measured on the P54, with static faraday multicollection that included monitors of potential interferences from Yb, Lu, Ta and W. Data are fractionation corrected to $^{178}Hf/^{177}Hf$ = 0.7215 and normalized to the average value of $^{176}Hf/^{177}Hf$ obtained for 11 to 13 measurements of the JMC-475 Hf standard made during the same analytical session as sample analyses. All data are reported relative to $^{176}Hf/^{177}Hf$ = 0.282160 for the JMC-475 standard. During the course of these measurements, values for $^{176}Hf/^{177}Hf$ for the JMC-475 standard ranged from 0.282124 to 0.282179. Errors quoted in Tables 2 and 3 for Hf isotopic compositions are in-run precisions reported as 2σ mean. External precision (all external precisions quoted as 2σ mean), based on the reproducibility of the standards run within an individual analytical session, is 0.0035%.

[21] Nd isotopic compositions for most Maymecha-Kotuy samples were measured on the P54 using a multidynamic program that measured all Nd isotopes as well as potential interferences from Ce and Sm. Data are fractionation corrected to $^{146}Nd/^{144}Nd$ = 0.7219 and reported relative to a value of $^{143}Nd/^{144}Nd$ = 0.511860 for the La Jolla Nd standard. The average value obtained for 29 runs of the La Jolla Nd standard over the course of the measurements reported here is 0.511831 ± 0.000009. All the kimberlite Nd isotopic data reported in Table 3 and Nd data for samples 3FG-19, 4FG-50 and 5FG-67 in Table 2 were measured on the DTM Thermo-Finnigan Triton using double Re filaments to produce a Nd+ ion beam. Data were measured statically in 9 faraday cups, monitoring Ce and Sm for correction of isobaric interferences and correcting for fractionation to $^{146}Nd/^{144}Nd$ = 0.7219. Average $^{143}Nd/^{144}Nd$ values for the La Jolla and JNdi Nd standards obtained during the course of the measurements reported here are 0.5118449 ± 0.0000013 (n = 5) and 0.5121051 ± 0.0000011 (n = 6), respectively. Because all in-run precisions were better than the external errors quoted above, the Nd data in Tables 2 and 3 are assigned the external precisions.

[22] Sr isotopic composition was determined by thermal ionization mass spectrometry (TIMS) using either a two-step multidynamic routine on the DTM VG-354 (most Maymecha-Kotuy samples) or statically on the Triton (all kimberlites and samples 3FG-19, 4FG-50, and 5FG-67) monitoring all Sr isotopes and ^{85}Rb, and correcting for fractionation to $^{86}Sr/^{88}Sr$ = 0.1194. During the period of the analyses reported here, the average $^{87}Sr/^{86}Sr$ obtained for the NIST-987 Sr standard was 0.710255 ± 0.000011 (n = 10) on the 354 and 0.710235 ± 0.000004 (n = 10) on the Triton. In-run precisions were always better than external reproducibility, so the Sr isotopic data in Tables 2

and 3 are assigned the external errors quoted above.

[23] Pb isotopic compositions were measured statically by TIMS using either the 354 (all Maymecha-Kotuy samples) or Triton (all kimberlites). On both instruments, Pb isotopic compositions show an external reproducibility controlled primarily by mass fractionation. On the 354, the average measured values for the NBS 981 Pb standard are $^{206}Pb/^{204}Pb$ = 16.927 ± 0.005, $^{207}Pb/^{204}Pb$ = 15.464 ± 0.006, and $^{208}Pb/^{204}Pb$ = 36.614 ± 0.021 (n = 9). On the Triton, the average values for these ratios are: 16.914 ± 0.016, 15.462 ± 0.022, 36.60 ± 0.07, (n = 6), respectively. All measured Pb isotopic compositions are corrected for mass fractionation on the basis of these average standard values compared to the isotopic composition of NBS 981 reported by *Todt et al.* [1996].

[24] Re and Os isotopic compositions were determined by negative-thermal-ionization mass spectrometry on the DTM 38 cm-radius mass spectrometer. Samples were loaded on Pt filaments in HBr, dried under heat lamp, and covered with $Ba(NO_3)_2$. Os was run as the OsO_3^- ion on the electron multiplier and fractionation corrected to $^{192}Os/^{188}Os$ = 3.80261. The average value for $^{187}Os/^{188}Os$ obtained for the DTM Os standard using this technique is 0.1742 ± 0.0002. Re was run as the ReO_4^- ion. Re and Os concentrations are precise to better than 0.5%.

4. Results

[25] Major- and trace-element data reported here for the Maymecha-Kotuy rocks overlap those of previous studies of this area [*Arndt et al.*, 1995; *Fedorenko and Czamanske*, 1997]. The Maymecha-Kotuy rocks show a very wide range in MgO concentration, from >40 wt% to <10 wt% with the MgO-rich compositions reflecting accumulation of olivine. The low-MgO members of the Maymecha-Kotuysuite are clearly distinguished by their lower SiO_2 and higher CaO and TiO_2 contents, compared to the more voluminous Siberian flood basalts (Figure 2). The compositional distinctions between the Siberian kimberlites and the high-Mg rocks in the Maymecha-Kotuy section are illustrated in Figure 2. The majority of high-Mg, Maymecha-Kotuy samples show little change in SiO_2 content (~40 wt%) between MgO concentrations of 15 and 40 wt%. The exceptions are the intrusive samples from the Kresty massif that have very high CaO and TiO_2 and low SiO_2 contents, reflecting the abundance of perovskite in these samples. On the plot of SiO_2 versus MgO, the kimberlites show decreasing SiO_2 with decreasing MgO, linking the meimechites with the perovskite-rich intrusive rocks. In most other major-element characteristics, the kimberlites follow the compositional trends defined by the extrusive mafic-alkalic rocks, and both extrapolate toward the fields defined by the more voluminous flood basalts. Exceptions notably include CaO, TiO_2 and K_2O, where both the Maymecha-Kotuy samples and the kimberlites show large increases in the abundance of these elements with decreasing MgO, forming trends that extrapolate to higher CaO, TiO_2 and K_2O than the majority of the flood basalts (Figure 2).

[26] The Maymecha-Kotuy mafic-alkalic rocks all show strong enrichment in the highly incompatible elements, with steep bulk-silicate-earth (BSE) normalized incompatible trace-element patterns (Figure 3) starting at Lu concentrations between 2 and 3 times BSE values and reaching maximum enrichments between 50 and 400 times BSE values for the most highly incompatible elements. Compared to elements of similar incompatibility, the range in K contents in the Maymecha-Kotuy rocks is relatively small, which suggests that the K content of the magmas was buffered by a potassic phase, likely phlogopite, during melting. Most samples have negative abundance anomalies at Pb and small positive abundance anomalies at Ta, but, with the exception of K, otherwise show generally smooth BSE-normalized, incompatible-element patterns. In this sense, the trace-element patterns are broadly similar to those of South African Group I kimberlites [*Le Roex et al.*, 2003] and a number of other mafic-alkalic rocks, such as those in central Brazil [e.g., *Gibson et al.*, 1995; *Carlson et al.*, 1996]. Though more enriched in highly incompatible elements than typical ocean-island basalts, the Maymecha-Kotuy samples have values of characteristic trace-element ratios, such as Ce/Pb and Ta/U, that are more similar to intraplate ocean-island basalts [*Hofmann et al.*, 1986] than to arc-related or subduction-influenced, mafic-alkalic rocks such as the lamproites and related rocks from Spain, Italy and Western Australia [*Nelson*, 1992].

[27] Sr, Nd and Hf isotopic compositions of both Maymecha-Kotuy and kimberlite samples extend the array seen for Siberian flood basalts to values approaching those of the depleted mantle, with

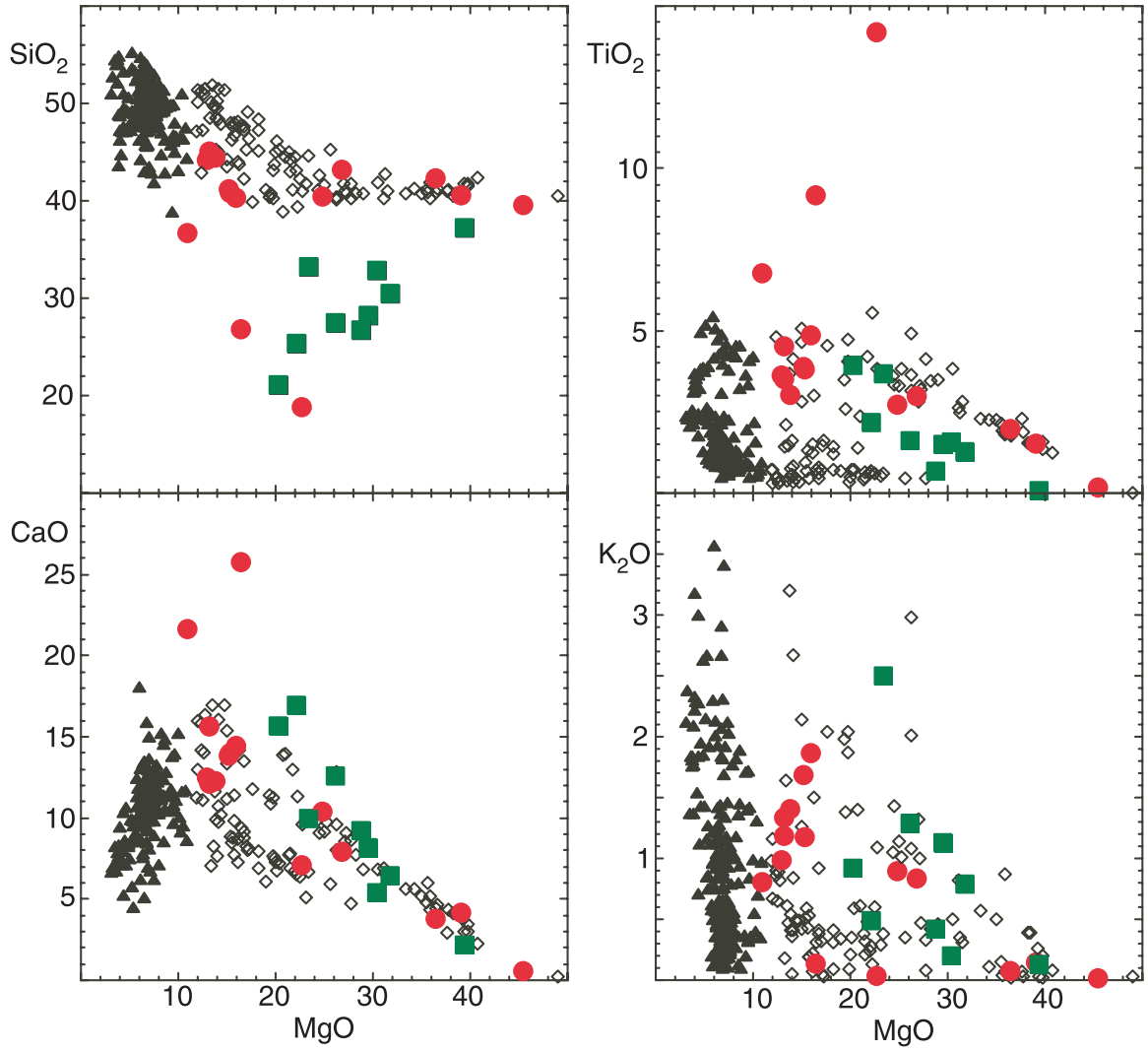

Figure 2. Major-element compositions of the studied Maymecha-Kotuy (red circles) and kimberlite (green squares) samples relative to the compositional range exhibited by the Siberian flood-volcanic data set contained in the GEOROC database, where the open black diamonds denote samples with MgO > 11 wt% and the filled black triangles denote samples with MgO < 11 wt%. The GEOROC data derive from the studies of *Lightfoot et al.* [1990], *Sharma et al.* [1991, 1992], *Sobolev et al.* [1992], *Hawkesworth et al.* [1993, 1995], *Wooden et al.* [1993], *Walker et al.* [1994, 1997], *Arndt et al.* [1995, 1998], *Basu et al.* [1995], *Horan et al.* [1995], and *Fedorenko and Czamanske* [1997].

initial ε_{Nd} and ε_{Hf} values as high as +7.2 and +10.8, respectively, and $^{87}Sr/^{86}Sr$ values as low as 0.70313 (Figure 4). The highest Nd and Hf isotopic compositions in the extrusive rocks are found in the meimechites, and the lowest values in the melilitites and mela-nephelinites. Initial Sr and Nd isotopic compositions are well correlated in the Maymecha-Kotuy samples and most kimberlites. Four kimberlites plot off the Sr-Nd array toward high $^{87}Sr/^{86}Sr$ values. Three of these samples have among the highest loss-on-ignition of the kimberlite data set, suggestive that the high $^{87}Sr/^{86}Sr$ values may reflect alteration and the addition of groundwater Sr. Hf and Nd isotopic compositions are well correlated in the Maymecha-Kotuy samples with the data falling within the array observed for intraplate, ocean-island basalts. Some kimberlites scatter at right angles to the Hf-Nd array defined by the Maymecha-Kotuy samples, with sample ES12/42 lying notably to the high ε_{Hf} side of the array.

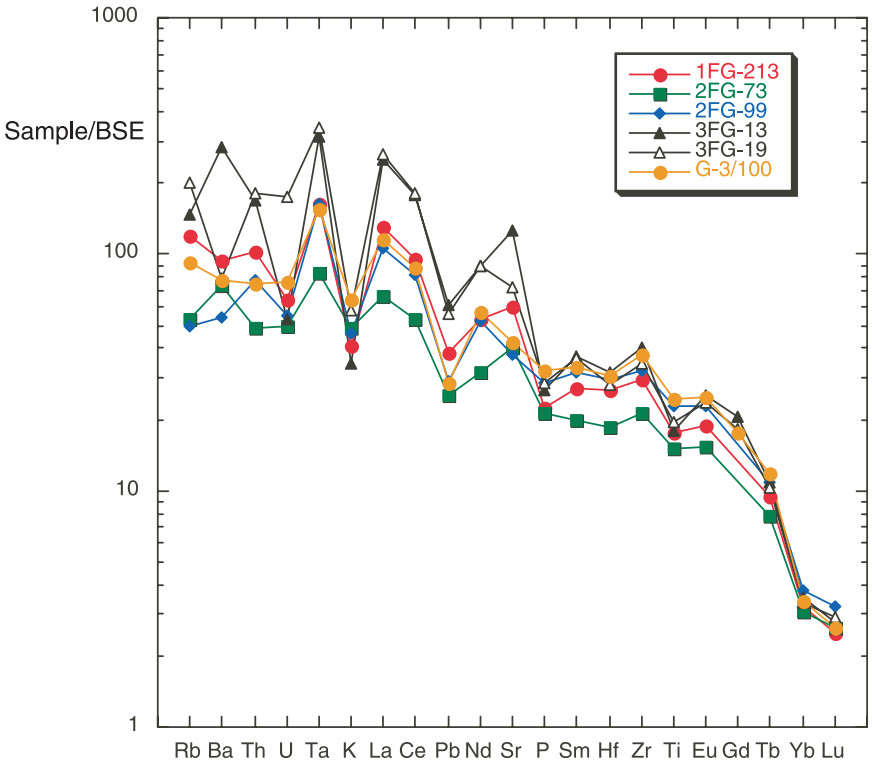

Figure 3. Incompatible trace-element patterns for the Maymecha-Kotuy samples, normalized to bulk-silicate earth (BSE) abundances [*McDonough and Sun*, 1995].

[28] Initial Os isotopic compositions range from 0.1193 to 0.1505, extending across the range observed for modern oceanic basalts to values just slightly higher and lower than seen in the basalts. Most of the meimechites and the ultramafic intrusive samples have initial $^{187}Os/^{188}Os$ values <0.1277, whereas the remaining samples all have initial $^{187}Os/^{188}Os$ values >0.137. Os isotopic variation correlates poorly, if at all, with other radiogenic isotopes, but does show some correlation with many major- and some trace-element abundances; the best correlations are between Os isotopic composition and Si, Mg, Na and Sc abundances (Figure 5).

[29] Measured Pb isotopic compositions are strongly influenced by U and Th decay since rock emplacement. For example, the three samples with $^{206}Pb/^{204}Pb > 24$ define a Pb-Pb isochron with an age of 253 ± 110 Ma, comparable to the eruption age of the samples. Most notable in this respect are the two samples from the Kresty intrusion that have high $^{206}Pb/^{204}Pb$ (26.56 and 38.1) and particularly high $^{208}Pb/^{204}Pb$ (120.9 and 224.3). When corrected using measured U/Pb ratios and a 251 Ma age, the uranogenic Pb isotopic composition of most Maymecha-Kotuy samples plot well within the range seen for Siberian flood basalts, albeit along the low $^{207}Pb/^{204}Pb$ side of the basalt data array (Figure 6). The Maymecha-Kotuy samples show a very limited range in $^{206}Pb/^{204}Pb$ compared to their range in Nd isotopic composition, whereas the kimberlites show very limited range in initial Nd isotopic composition, but a wider range in $^{206}Pb/^{204}Pb$ than the Maymecha-Kotuy samples. The range in initial Pb isotopic composition of the kimberlites may reflect alteration-induced changes to their U/Pb ratios. A line fit through the majority of Maymecha-Kotuy and kimberlite data on the $^{207}Pb/^{204}Pb$ vs. $^{206}Pb/^{204}Pb$ plot (Figure 6) corresponds to an age of approximately 950 Ma.

[30] Radiogenic isotopic compositions in the Maymecha-Kotuy rocks correlate poorly, if at all, with trace-element ratios such as Ce/Pb or Th/Ta. For these ratios, the Maymecha-Kotuy rocks fall within the field defined by ocean ridge and ocean island basalts, unlike the majority of Siberian flood basalts that scatter to higher Th/Ta and lower Ce/Pb (Figure 7). Nd, and to a lesser extent Os, isotopic

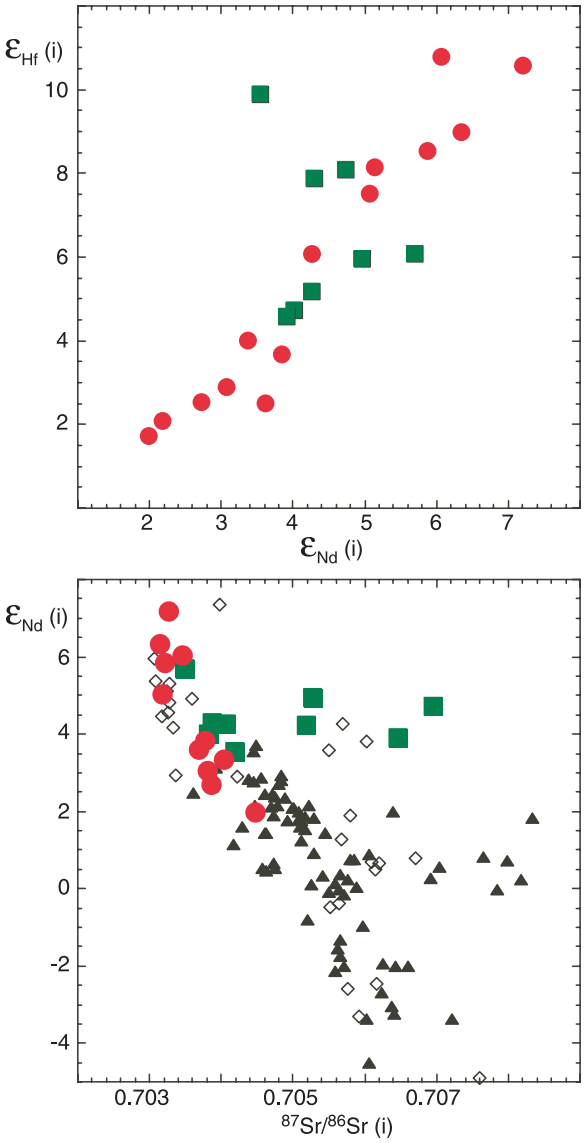

Figure 4. Initial Sr, Nd, and Hf isotopic compositions of the studied Maymecha-Kotuy (red circles) and kimberlite (green squares) samples and the GEOROC Siberian flood-volcanic data set (MgO > 11%, open diamonds; MgO < 11%, black triangles) from the data sources listed in the caption to Figure 2.

composition shows some correlation with Tb/Yb ratio (Figure 7).

5. Discussion

[31] High-Mg, often incompatible-element-rich, magmas have now been found in association with several flood-volcanic provinces, including the Letaba Formation of the Karoo basalts [*Ellam et al.*, 1992], the picrites of the early phase of the North Atlantic Igneous Province [*Saunders et al.*, 1997], and the mafic-alkalic rocks in the Narmada Lineament of the Deccan Province [*Mahoney*, 1988]. Whether these magmas can be used to extract information on the petrogenesis of the more typical, and more voluminous, tholeiitic basalts of flood-basalt provinces has been a subject of some discussion [e.g., *Ellam and Cox*, 1991; *Arndt et al.*, 1998]. The mafic-alkalic magmas offer the advan-

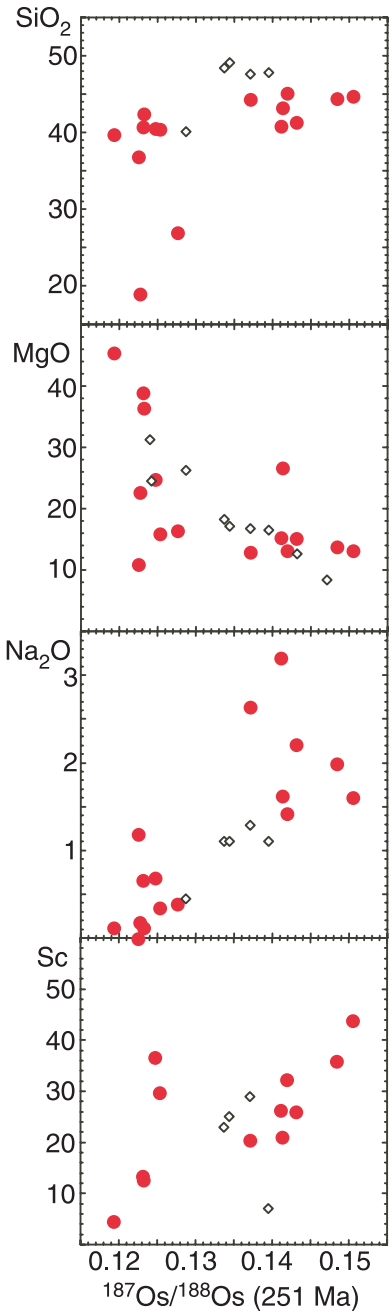

Figure 5. Variation in age-corrected Os isotopic compositions of Maymecha-Kotuy samples. Additional data (black diamonds) from *Horan et al.* [1995].

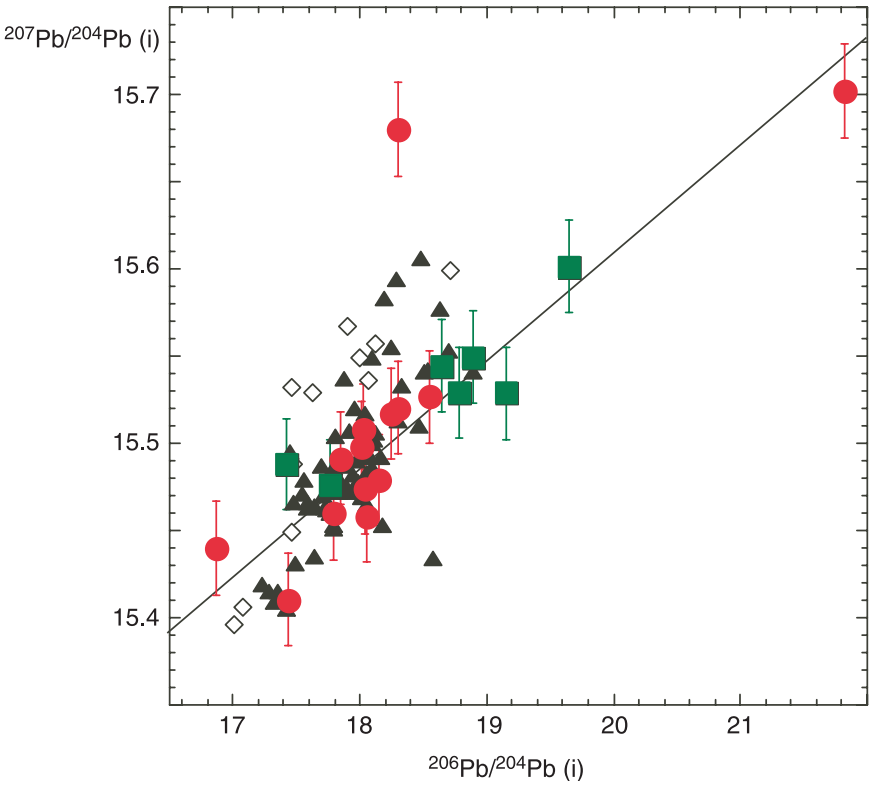

Figure 6. Age-corrected uranogenic Pb isotopic compositions for the studied Maymecha-Kotuy (red circles) and kimberlite (green squares) samples and other Siberian flood-volcanic rocks from the GEOROC database (MgO > 11%, black diamonds; MgO < 11%, black triangles) with data sources given in the caption to Figure 2. The line shows a slope corresponding to 950 Ma.

tage that many of their chemical features (e.g., high Mg number and high Ni content) suggest that they are near primary melts of the mantle and have not experienced the crustal-level fractionation that has modified the composition of most flood basalts [*Carlson*, 1991]. Flood basalts, however, tend to have relatively high abundances of the heavy REE, and hence low Tb/Yb (Figure 7), a sign that garnet was not a residual phase during the melting that produced the basalts. In turn, this is suggestive of relatively shallow (<100 km) melting depths for the basalts. In contrast, the heavy REE depletion (high Tb/Yb, Figure 7) and strong light REE enrichment of the mafic-alkalic magmas indicate that they likely formed by small degrees of melting of a source that contained garnet. This inference is consistent with experimental evidence indicating that ultramafic-alkalic magmas can be generated by low-degree melting of carbonated peridotite at depths of 150–200 km [*Herzberg and Zhang*, 1996; *Dalton and Presnall*, 1998; *Gudfinnsson and Presnall*, 2005; *Keshav et al.*, 2005; *Elkins-Tanton et al.*, 2006] and possibly much deeper [*Ringwood et al.*, 1992]. The possibility that phlogopite was a residual phase during melting, as suggested by the limited range in K contents of the Maymecha-Kotuy samples, suggests that the melt last equilibrated at the shallower end of this range, within the stability field of phlogopite.

[32] As has been pointed out previously [*Arndt et al.*, 1998], the Sr and Nd isotopic compositions of the meimechites overlap those of typical ocean-island basalts, as do key incompatible-trace-element ratios such as Th/Ta and Ce/Pb (Figure 7). The low $^{87}Sr/^{86}Sr$ and high $^{143}Nd/^{144}Nd$ values of the meimechites are consistent with a source that is moderately depleted in incompatible elements. Starting from an incompatible-element-depleted source, reaching the very high incompatible-element contents of the Maymecha-Kotuy rocks can only be achieved by very low degrees of melting. For example, the incompatible-element concentrations of the Maymecha-Kotuy rocks can be matched by 1% partial melting of a mantle source with incompatible-element abundances similar to bulk-silicate earth (BSE) estimates

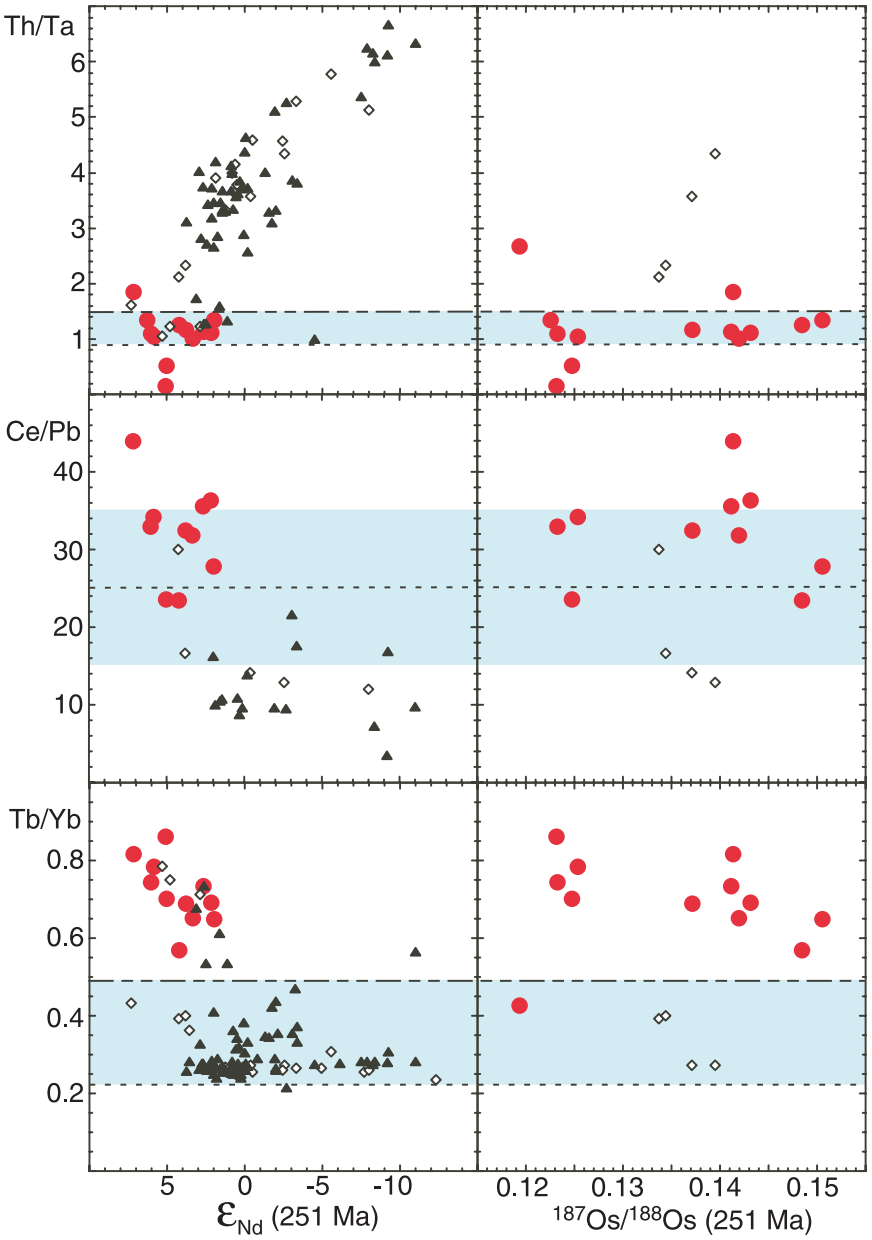

Figure 7. Comparison of trace-element ratio variation with initial Nd and Os isotopic composition. Maymecha-Kotuy samples are shown by the red circles. Siberian flood-volcanism data from GEOROC shown by the open black diamonds (samples with MgO > 11%) and filled black triangles (samples with MgO < 11%). The blue bands in each figure show the range between the average trace-element ratio of MORB (dotted line) and OIB (dot-dash line) from *Sun and McDonough* [1989].

[*McDonough and Sun*, 1995], but require melt fractions of only 0.1% if the mantle source is highly depleted in incompatible elements, such as that proposed for the source of mid-ocean-ridge basalts [*Salters and Stracke*, 2004]. A mantle composition only mildly depleted in incompatible elements compared to BSE estimates, with Sr, Nd and Hf isotopic compositions similar to those measured for the Maymecha-Kotuy samples, for example, the early-depleted mantle reservoir modeled by *Boyet and Carlson* [2005], would require on the order of 0.5% partial melting to produce the trace-element abundances of these samples. Recent experimental work [*Gudfinnsson and Presnall*, 2005] suggests that kimberlitic composition melts can be formed by 0.6–0.7% melting, with melili-

titic compositions requiring higher amounts of melting.

[33] The Os isotopic compositions of the Maymecha-Kotuy samples show rough correlations with major- and some trace-element variations (Figure 5), and Nd isotopic compositions are somewhat correlated with Tb/Yb ratios (Figure 7). The fact that the radiogenic isotopic compositions correlate with major- and trace-element characteristics of the lavas shows that the compositional variation is not simply the result of varying degrees of melting of a homogeneous source. The high MgO, low SiO_2, Na_2O and Sc end of the correlations with Os isotopic variation is characterized by Os isotopic compositions mostly within the range expected for the convecting mantle (~0.128 at 251 Ma) [*Walker et al.*, 2002] with one sample (4FG-32) at the low end of this range approaching values found for old, Re-depleted, lithospheric mantle [*Carlson et al.*, 2005]. At the low MgO and high Na_2O and Sc end of these correlations, the samples have $^{187}Os/^{188}Os$ well above that typical of mantle peridotite, but within the range seen for modern ocean-island basalts [*Reisberg et al.*, 1993]. A similar relation between compositional characteristics and Os isotopic composition has been observed in other mafic-alkalic provinces [*Carlson et al.*, 1996; *Carlson and Nowell*, 2001]. A likely explanation for the compositional and Os isotopic range observed in the Maymecha-Kotuy samples is that they sample mantle end-members that range from pure peridotite (low $^{187}Os/^{188}Os$ end-member) to a mixture of peridotite plus pyroxene-rich components such as pyroxenite and/or eclogite "veining" in a peridotite matrix. Because most melts have higher Re/Os ratios than peridotite, the pyroxene-rich component in the mantle, whether derived from the crystallization of infiltrating magmas or by recycling of subducted basaltic crust, likely will have higher Re/Os, and hence with time, higher $^{187}Os/^{188}Os$, than peridotite.

[34] The fact that Nd and Os isotopic compositions do not correlate with ratios such as Ce/Pb and Th/Ta (Figure 7) shows that neither isotopic end-member contains the chemical characteristics associated with continental crust or continent-derived sediments. The very high Tb/Yb of the Maymecha-Kotuy rocks is consistent with the presence of residual garnet during melting, because garnet is the only mantle phase that can cause such dramatic fractionation between middle and heavy REE. The Tb/Yb correlation with Nd isotopic composition and, to a lesser extent, Os isotopic composition could be explained by decreasing amounts of modal garnet in the low $^{143}Nd/^{144}Nd$ end-member. The fact that Tb/Yb shows no correlation with the abundances of highly incompatible trace elements (e.g., Ba, Th, La), but some correlation with garnet-compatible elements such as Sc, supports this possibility.

[35] Nd and Hf model ages for most samples are in the range of 400–800 Ma (Table 2), but these likely underestimate the time when the compositionally distinct sources were generated due to Sm/Nd and Lu/Hf fractionation during melting. The ~950 Ma slope in the $^{207}Pb/^{204}Pb$ vrs $^{206}Pb/^{204}Pb$ (Figure 6) is less sensitive to disturbance by partial melting than the Sm/Nd and Lu/Hf systems, and is consistent with the idea that the geochemical heterogeneity present within the source of the Maymecha-Kotuy samples has been present since at least the late-Proterozoic. Whether or not this source "age" reflects the time of a discrete event in the history of the sub-Siberian mantle or simply reflects the normal chemical and isotopic heterogeneity existing in the convecting mantle is not resolved by this data set.

[36] An important point to note for any model attempting to explain the compositional variability in the source of the Maymecha-Kotuy magmas is that the isotopic and trace-element ratio systematics of the Maymecha-Kotuy samples argue strongly that the source of the magmas did not contain foundering continental lithosphere or subducted crustal materials [*Elkins-Tanton et al.*, 2006]. The relatively high $^{143}Nd/^{144}Nd$ and $^{176}Hf/^{177}Hf$ values, and low $^{87}Sr/^{86}Sr$ values characteristic of the Maymecha-Kotuy rocks rule out a significant "crustal" component in these magmas regardless of whether the "crustal" component is introduced directly by wall rock contamination of the magmas as they penetrated the continental crust or whether the crustal materials were introduced into the mantle below this area by subduction or by delamination of the overlying lower crust. This inference is supported by key incompatible-element ratios such as Ce/Pb and Th/Ta (Figure 7) in the Maymecha-Kotuy samples that are within the range observed for ocean-island basalts [*Hofmann et al.*, 1986] and distinct from either convergent margin rocks or continental lamproites that appear to have a source in mantle contaminated by recycled crustal materials [*Fraser et al.*, 1986; *Nelson*, 1992]. Similarly, because the Maymecha-Kotuy samples have isotopic compositions that overlap those of the kimberlites that were erupted well before, and well after,

the flood-volcanic event, the mantle supplying Maymecha-Kotuy magmatism need not have been modified by events temporally associated with the flood-volcanic event, such as the arrival of a mantle plume or delamination of a section of continental lithosphere.

[37] The isotopic range of the Maymecha-Kotuy samples overlaps the isotopic variation seen in intraplate ocean-island basalts (OIB). The low $^{187}Os/^{188}Os$ end of the array is most like the ocean island basalt component variably called FOZO [*Hart et al.*, 1992], "C" [*Hanan and Graham*, 1996], or "PHEM" [*Farley et al.*, 1992] that is the component of OIB characterized by the highest $^{3}He/^{4}He$ [*Class and Goldstein*, 2005]. $^{3}He/^{4}He$ measurements [*Basu et al.*, 1995] of a single olivine-nephelinite from the Maymecha-Kotuy section provide evidence for a high $^{3}He/^{4}He$ source for these magmas (>12.7 times atmospheric $^{3}He/^{4}He$). Lower values measured for meimechites were interpreted as reflecting outgassing and a contribution of radiogenic ^{4}He, and thus thought not to track source He isotopic compositions [*Basu et al.*, 1995]. Conventionally, the upper mantle or asthenosphere is interpreted to have the composition of the mantle that supplies mid-ocean ridge basalts [*Zindler and Hart*, 1986]. The near complete lack of the strongly incompatible-element-depleted signature characteristic of the source of MORB in magmas not erupted along ocean ridges has given rise to alternative models that suggest that the MORB source is formed either by previous melting of more fertile mantle [*Phipps Morgan and Morgan*, 1998], or that the MORB source is a heterogeneous mixture of mostly a depleted matrix with small amounts of enriched, and more easily melted, material [*Ito and Mahoney*, 2006]. In this mixed-source model, MORB is produced by high-degree melting under the thin lithosphere of an ocean ridge, where more limited melting of a similar source under thicker lithosphere preferentially samples the more enriched components [*Ito and Mahoney*, 2006]. This latter explanation is consistent with the evidence from the Maymecha-Kotuy rocks that one end-member is a peridotite with high $^{143}Nd/^{144}Nd$ and low $^{87}Sr/^{86}Sr$, and another end-member is more pyroxene-rich, with lower Nd and higher Sr isotopic composition. The low degrees of melting that produced both the Maymecha-Kotuy and Siberian kimberlites may have preferentially sampled the more compositionally extreme end-members in such a heterogeneous source in comparison to the larger-volume volcanism associated with the flood basalts. The fact that similar isotopic compositions are found in the Siberian kimberlites suggests that this type of mantle has been present in the mantle beneath Siberia for at least the last half-billion years, which is not surprising if it is a major compositional component of the convecting mantle

5.1. Relation to Flood-Volcanic Activity

[38] Most of the Siberian flood basalts have lower $^{143}Nd/^{144}Nd$ and higher $^{87}Sr/^{86}Sr$ values than the high-MgO Maymecha-Kotuy samples [e.g., *Lightfoot et al.*, 1990; *Sharma et al.*, 1991; *Wooden et al.*, 1993]. This distinction between the basalts and the mafic-alkalic rocks could reflect either a larger percentage of the pyroxene-rich component present in the Maymecha-Kotuy source, or crustal contamination of the basalts. These two possibilities would be accompanied by quite different trace-element expressions. Extrapolating the correlations between Os isotopic composition and major-element composition observed in the Maymecha-Kotuy rocks to the composition of the typical Siberian flood basalt would predict radiogenic Os isotopic compositions ($^{187}Os/^{188}Os > 0.13$). If our interpretation of the cause of Os isotopic variation is correct, this would also suggest that the source of the flood basalts was rich in "olivine-poor" components. A pyroxene-rich source for flood basalts is a not uncommon proposition [*Wright et al.*, 1989; *Campbell and Griffiths*, 1990; *Cordery et al.*, 1997]. Os isotopic measurements on flood basalts are difficult, at best, because of their commonly low Os concentrations [*Molzahn et al.*, 1996; *Hart et al.*, 1997; *Chesley and Ruiz*, 1998]. Os isotopic data for Siberian flood basalts were obtained from measurements of platinum-group-element-rich intrusions where the initial $^{187}Os/^{188}Os$ ranges from 0.128 to 0.144 [*Walker et al.*, 1994], overlapping the range seen here for the lower MgO Maymecha-Kotuy samples. Thus these data do not strongly point to a pyroxene-dominated mantle source for the flood-basalt lavas that was distinct from the source of the Maymecha-Kotuy rocks. Instead, the low Ce/Pb and high Th/Ta of the flood basalts and the correlation of these ratios with isotopic composition (Figure 7) are the expected result of crustal contamination of primitive magmas similar to those of the Maymecha-Kotuy samples.

[39] Unless the Siberian flood basalts were derived from a source completely unrelated to that sampled by the Maymecha-Kotuy magmas, the data presented here suggest that the primary flood-basalt

magmas had isotopic compositions well within the range of typical intraplate OIB. The evolution from flood basalts characterized by high $^{87}Sr/^{86}Sr$ and low $^{143}Nd/^{144}Nd$ values to lower $^{87}Sr/^{86}Sr$ and higher $^{143}Nd/^{144}Nd$ values in both pre- and post-flood-basalt activity in a given province is a characteristic displayed by many flood-basalt provinces, as is the eventual arrival at a FOZO-like composition [*Carlson*, 1991]. While this could reflect a compositionally distinct plume contribution to flood-basalt magma, the alternative, which we consider more likely, is that the very high magma production and transport rates present during the peak of a flood-basalt episode sufficiently raise the temperature of the continental lithosphere, through which the flood-basalt magmas must penetrate, such that assimilation of lithospheric material, both as small-volume melts of lithospheric mantle [*Ellam and Cox*, 1991] and more directly through wall rock assimilation in crustal magma chambers becomes commonplace. At lower magma production rates, both preceding and following the main pulse of activity, the lithosphere can cool sufficiently so that it no longer contributes significantly to sub-lithospheric melts, allowing a broader compositional spectrum of sub-lithospheric melts to erupt, as appears to have happened in the Maymecha-Kotuy region. The low percentage of melt, the great depths of melting, and the lack of a lithospheric signature in the Maymecha-Kotuy samples also may reflect the fact that this activity took place on the northeastern margin of the Siberian flood-volcanic province in an area marginal to the area of maximum volcanic output.

5.2. Implications for the Cause of Siberian Magmatism

[40] Flood-basalt volcanism has been attributed to continental extension [*Harry and Leeman*, 1995], to the effects of mantle flow around lithospheric mantle boundaries [*Carlson and Hart*, 1987; *King and Anderson*, 1998], mantle plumes [e.g., *Duncan*, 1978; *Richards et al.*, 1989; *White and McKenzie*, 1989], and by delamination of the lower parts of continental lithosphere [e.g., *Kay and Kay*, 1993; *Elkins-Tanton and Hager*, 2000; *Hales et al.*, 2005]. In plume models, uplift is expected to precede eruption and persist for a period of time. In lithosphere delamination models, subsidence should precede volcanism, but uplift during and after volcanism is expected [*Kay and Kay*, 1993; *Elkins-Tanton and Hager*, 2000]. The overall subsidence history of the Siberian flood-volcanic province argues against both of these mechanisms for instigation of the flood volcanism.

[41] *Czamanske et al.* [1998] presented comprehensive paleogeographic and paleotectonic reconstructions from the prevolcanic and volcanic record which show that the central and eastern portion of the Siberian flood-volcanic province, comprising a combined thickness of ~6500 m of volcanic rocks, was undergoing well-compensated subsidence before and during the flood-volcanic event. These reconstructions show conclusively that there was no plume-relatable, surficial uplift within this broad region of present-day, flood-volcanic exposure.

[42] To the west of the present-day flood-volcanic exposures on the Siberian craton lies the Western Siberian Basin (WSB) in which oil and gas boreholes have sampled basaltic rocks at depths of 2620 to 7006 m. These basaltic rocks have been shown to be coeval with, and chemically equivalent to, lower units of the well-studied sequence near Noril'sk [*Reichow et al.*, 2005]. *Saunders et al.* [2005] argue that plume-related uplift associated with Siberian flood volcanism may have been centered over the WSB, but they show a record only of post-Permian subsidence in the WSB with no clear evidence for pre-flood-volcanism uplift. We find it remarkable that as much as 2 km of uplift could be proposed for Permian rocks now sporadically sampled at depths of thousands of meters in a basin that has been rifting and subsiding since the Late Permian. *Saunders et al.* [2005] assume that the bulk of the rifting took place in the basin in the Late Permian or Triassic and that rapid subsidence commenced at ~250 Ma, and continued at a lesser rate through the Cenozoic, by which time ~2.5 km of subsidence had occurred. They fail to deal with the fact that none of the basaltic rocks present at depth in the WSB correlate with the voluminous Upper series basalts (~2400 m thick) of the Noril'sk area, which increase in thickness to the northeast, i.e., away from the WSB [*Wooden et al.*, 1993, Figure 3c]. Moreover an additional 3000-m thickness of coeval volcanic rocks, not present either in the WSB or at Noril'sk, is present in the Maymecha-Kotuy region, some 1000 km east of the center of the WSB.

[43] The isotopic characteristics presented here for the Maymecha-Kotuy rocks demonstrate the presence in the mantle beneath Siberia of material with isotopic composition overlapping a common component observed in intraplate OIB. The fact that the isotopic compositions of the Siberian kimberlites

overlaps those of the Maymecha-Kotuy rocks shows that these compositions have been present in the mantle beneath Siberia for at least 475 Ma, the age of the oldest kimberlite analyzed. This indicates that it is not necessary to appeal to a deep-mantle source (e.g., a plume) in order to obtain material with these compositional characteristics. The record of continuous subsidence of the Siberian Traps during the Permo-Triassic, accompanied by rifting along the West Siberian Basin, and the proximity of the flood-volcanism to the craton margin are consistent with the "edge-effect" mantle flow model of *King and Anderson* [1998] where the ultimate source of the magmas is the convecting mantle beneath Siberia.

Acknowledgments

[44] John Mahoney and Rob Ellam provided two detailed reviews of the original manuscript. We thank these reviewers for their insightful comments, and their very useful suggestions for improving the clarity of our presentation, even if we were not able to answer all the questions raised. We also thank Vince Salters for his very efficient handling of the paper. This work was supported by NSF grant EAR-0106475.

References

Agashev, A. M., Y. Orihashi, T. Watanabe, N. P. Pokhilenko, and V. P. Serenko (2000), Isotope-geochemical features of the Siberian-platform kimberlites in connection with the problem of their origin (in Russian), *Geol. Geofiz.*, *41*, 90–99.

Arndt, N., C. Chauvel, G. Czamaske, and V. Fedorenko (1998), Two mantle sources, two plumbing systems: Tholeiitic and alkaline magmatism of the Maymecha River basin, Siberian flood volcanic province, *Contrib. Mineral. Petrol.*, *133*, 297–313.

Arndt, N., K. Lehnert, and Y. Yasil'ev (1995), Meimechites: Highly magnesian lithosphere-contaminated alkaline magmas from deep subcontinental mantle, *Lithos*, *34*, 41–59.

Baedecker, P. A. (Ed.) (1987), *Methods for Geochemical Analysis*, *U.S. Geol. Surv. Bull.*, *1770*, Reston, Va.

Basu, A. R., R. J. Poreda, P. R. Renne, F. Teichmann, Y. R. Vasiliev, N. V. Sobolev, and B. D. Turrin (1995), High-^{3}He plume origin and temporal-spatial evolution of the Siberian flood basalts, *Science*, *269*, 822–825.

Bobrievich, A. P., I. P. Ilupin, I. T. Kozlov, L. I. Lebedeva, A. A. Pankratov, G. I. Smirnov, A. D. Kharkiv (1964), Petrography and mineralogy of the kimberlite rocks of Yakutia, 191 pp., Nedra, Moscow.

Boyet, M., and R. W. Carlson (2005), ^{142}Nd evidence for early (>4.53 Ga) global differentiation of the silicate Earth, *Science*, *309*, 576–581.

Campbell, I. H., and R. W. Griffiths (1990), Implications of mantle plume structure for the evolution of flood basalts, *Earth Planet. Sci. Lett.*, *99*, 79–93.

Carlson, R. W. (1991), Physical and chemical evidence on the cause and source characteristics of flood basalt volcanism, *Aust. J. Earth Sci.*, *38*, 525–544.

Carlson, R. W., and W. K. Hart (1987), Crustal genesis on the Oregon Plateau, *J. Geophys. Res.*, *92*, 6191–6206.

Carlson, R. W., and G. M. Nowell (2001), Olivine-poor sources for mantle-derived magmas: Os and Hf isotopic evidence from potassic magmas of the Colorado Plateau, *Geochem. Geophys. Geosyst.*, *2*(6), doi:10.1029/2000GC000128.

Carlson, R. W., G. W. Lugmair, and J. D. Macdougall (1981), Columbia River volcanism: The question of mantle heterogeneity or crustal contamination, *Geochim. Cosmochim. Acta*, *45*, 2483–2499.

Carlson, R. W., S. Esperanca, and D. P. Svisero (1996), Chemical and Os isotopic study of Cretaceous potassic rocks from southern Brazil, *Contrib. Mineral. Petrol.*, *125*, 393–405.

Carlson, R. W., D. G. Pearson, and D. E. James (2005), Physical, chemical, and chronological characteristics of continental mantle, *Rev. Geophys.*, *43*, RG1001, doi:10.1029/2004RG000156.

Chesley, J. T., and J. Ruiz (1998), Crust-mantle interaction in large igneous provinces: Implications from the Re-Os isotope systematics of the Columbia River flood basalts, *Earth Planet. Sci. Lett.*, *154*, 1–11.

Class, C., and S. L. Goldstein (2005), Evolution of helium isotopes in the Earth's mantle, *Nature*, *436*, 1107–1112.

Cordery, M. J., G. F. Davies, and I. H. Campbell (1997), Genesis of flood basalts from eclogite-bearing mantle plumes, *J. Geophys. Res.*, *102*, 20,179–20,197.

Czamanske, G. K., A. B. Gurevitch, V. Fedorenko, and O. Simonov (1998), Demise of the Siberian plume: Paleogeographic and paleotectonic reconstruction from the prevolcanic and volcanic record, north-central Siberia, *Int. Geol. Rev.*, *40*, 95–115.

Dalton, J. A., and D. C. Presnall (1998), The continuum of primary carbonatitic-kimberlitic melt compositions in equilibrium with lherzolite: Data from the system CaO-MgO-Al_2O_3–SiO_2–CO_2 at 6 GPa, *J. Petrol.*, *39*, 1953–1964.

Davis, G. L., N. V. Sobolev, and A. D. Kharkiv (1980), New data about the age of the Yakutian kimberlites obtained from zircon by the U-Pb method (in Russian), *Dokl. Akad. Nauk SSSR*, *254*, 175–179.

Duncan, R. A. (1978), Geochronology of basalts from the Ninetyeast Ridge and continental dispersion in the eastern Indian Ocean, *J. Volcanol. Geotherm. Res.*, *4*, 283–305.

Elkins-Tanton, L. T., and B. H. Hager (2000), Melt intrusion as a trigger for lithospheric foundering and the eruption of the Siberian flood basalt, *Geophys. Res. Lett.*, *27*, 3937–3940.

Elkins-Tanton, L. T., D. S. Draper, C. B. Agee, J. Jewell, A. Thorpe, and P. C. Hess (2006), The last lavas of the Siberian flood basalts: Results from experimental petrology, *Contrib. Mineral. Petrol.*, in press.

Ellam, R. M., and K. G. Cox (1991), An interpretation of Karoo picrite basalts in terms of interaction between asthenospheric magmas and the mantle lithosphere, *Earth Planet. Sci. Lett.*, *105*, 330–342.

Ellam, R. M., R. W. Carlson, and S. B. Shirey (1992), Evidence from Re-Os isotopes for plume-lithosphere mixing in Karoo flood basalt genesis, *Nature*, *359*, 718–721.

Farley, K. A., J. Natland, and H. Craig (1992), Binary mixing of enriched and undegassed (primitive?) mantle components (He, Sr, Nd, Pb) in Samoan lavas, *Earth Planet. Sci. Lett.*, *111*, 183–199.

Fedorenko, V., G. Czamanske, T. Zen'ko, J. Budahn, and D. Siems (2000), Field and geochemical studies of the melilite-bearing Arydzhangsky Suite, and an overall perspective on the Siberian alkaline-ultramafic flood volcanic rocks, *Int. Geol. Rev.*, *42*, 769–804.

Fedorenko, V. A., and G. K. Czamanske (1997), Results of new field and geochemical studies of the volcanic and intrusive rocks of the Maymecha-Kotuy area, Siberian flood basalt province, Russia, *Int. Geol. Rev.*, *39*, 479–531.

Fedorenko, V. A., P. C. Lightfoot, A. J. Naldrett, G. K. Czamanske, C. J. Hawkesworth, J. L. Wooden, and D. S. Ebel (1996), Petrogenesis of the Siberian flood-basalt sequence at Noril'sk, *Int. Geol. Rev.*, *32*, 99–135.

Fraser, K. J., C. J. Hawkesworth, A. J. Erlank, R. H. Mitchell, and B. H. Scott-Smith (1986), Sr, Nd, and Pb isotope and minor element geochemistry of lamproites and kimberlites, *Earth Planet. Sci. Lett.*, *76*, 57–70.

Gibson, S. A., R. N. Thompson, O. H. Leonardos, A. P. Dicken, and J. B. Mitchell (1995), The late Cretaceous impact of the Trindade mantle plume: Evidence from large-volume, mafic, potassic magmatism in SE Brazil, *J. Petrol.*, *36*, 189–229.

Golubeva, Y. Y., and A. I. Tsepin (2004), Petrochemical and mineralogical constraints for diagnostics of Yakutian kimberlites, *Dokl. Earth Sci.*, *397*, 798–803.

Gudfinnsson, G. H., and D. C. Presnall (2005), Continuous gradations among primary carbonatitic, kimberlitic, melilititic, basaltic and komatiitic melts in equilibrium with garnet lherzolite at 3–8 GPa, *J. Petrol.*, *46*, 1645–1659.

Hales, T. C., D. L. Abt, E. D. Humphreys, and J. J. Roering (2005), A lithospheric instability origin for Columbia River flood basalts and Wallowa Mountains uplift in northeast Oregon, *Nature*, *438*, 842–845.

Hanan, B., and D. Graham (1996), Lead and helium isotope evidence from oceanic basalts for a common deep source of mantle plumes, *Science*, *272*, 991–995.

Harry, D. L., and W. P. Leeman (1995), Partial melting of melt metasomatized subcontinental mantle and the magma source potential of the lower lithosphere, *J. Geophys. Res.*, *100*, 10,255–10,269.

Hart, S. R., E. H. Hauri, L. A. Oschmann, and J. A. Whitehead (1992), Mantle plumes and entrainment: Isotopic evidence, *Science*, *256*, 517–520.

Hart, W. K., R. W. Carlson, and S. B. Shirey (1997), Radiogenic Os in primitive basalts from the northwestern U.S.A.: Implications for petrogenesis, *Earth Planet. Sci. Lett.*, *150*, 103–116.

Hawkesworth, C. J., P. C. Lightfoot, J. M. Hergt, A. J. Naldrett, N. S. Gorbachev, V. A. Fedorenko, and W. Doherty (1993), Remobilization of the continental lithosphere by a mantle plume: Trace element and Sr-, Nd-, and Pb-isotope evidence from picritic and tholeiitic lavas of the Noril'sk district, Siberian traps, *Contrib. Mineral. Petrol.*, *114*, 171–188.

Hawkesworth, C. J., P. C. Lightfoot, V. A. Fedorenko, S. Blake, A. J. Naldrett, W. Doherty, and N. S. Gorbachev (1995), Magma differentiation and mineralisation in the Siberian flood basalts, *Lithos*, *34*, 61–88.

Herzberg, C., and J. Zhang (1996), Melting experiments on anhydrous peridotite KLB-1: Compositions of magmas in the upper mantle and transition zone, *J. Geophys. Res.*, *101*, 8271–8295.

Hofmann, A. W., K. P. Jochum, M. Seufert, and W. M. White (1986), Nb and Pb in oceanic basalts: New constraints on mantle evolution, *Earth Planet. Sci. Lett.*, *79*, 33–45.

Horan, M. F., R. J. Walker, V. A. Fedorenko, and G. K. Czamanske (1995), Osmium and neodymium isotopic constraints on the temporal and spatial evolution of Siberian flood basalt sources, *Geochim. Cosmochim. Acta*, *59*, 5159–5168.

Ilupin, I. P. (1981), Relation between kimberlites and other rocks and the problems of kimberlite magma genesis, *Dokl. Akad. Nauk SSSR*, *261*, 1198–1202.

Ito, G., and J. J. Mahoney (2006), Melting a high $^3He/^4He$ source in a heterogeneous mantle, *Geochem. Geophys. Geosyst.*, *7*, Q05010, doi:10.1029/2005GC001158.

Kamo, S. L., G. K. Czamanske, and T. E. Krogh (1996), A minimum U-Pb age for Siberian flood-basalt volcanism, *Geochim. Cosmochim. Acta*, *60*, 3505–3511.

Kamo, S. L., G. K. Czamanske, Y. Amelin, V. A. Fedorenko, and V. R. Trofimov (2003), Rapid eruption of Siberian flood-volcanic rocks and evidence for coincidence with the Permian-Triassic boundary and mass extinction at 251 Ma, *Earth Planet. Sci. Lett.*, *214*, 75–91.

Kay, R. W., and S. M. Kay (1993), Delamination and delamination magmatism, *Tectonophysics*, *219*, 177–189.

Keshav, S., A. Corgne, G. H. Gudfinnsson, M. Bizimis, W. F. McDonough, and Y. Fei (2005), Kimberlite petrogenesis: Insights from clinopyroxene-melt partitioning experiments at 6 GPa in the CaO-MgO-Al_2O_3–CO_2 system, *Geochim. Cosmochim. Acta*, *69*, 2829–2845.

King, S. D., and D. L. Anderson (1998), Edge-driven convection, *Earth Planet Sci. Lett.*, *160*, 289–296.

Komarov, A. N., and I. P. Ilupin (1990), Geochronology of kimberlites of the Siberian Platform by the fission-track method (in Russian), *Geokhimiya*, *3*, 365–372.

Le Roex, A. P., D. R. Bell, and P. Davis (2003), Petrogenesis of Group 1 kimberlites from Kimberley, South Africa: Evidence from bulk-rock geochemistry, *J. Petrol.*, *44*, 2261–2286.

Lightfoot, P. C., A. J. Naldrett, N. S. Gorbachev, W. Doherty, and V. A. Fedorenko (1990), Geochemistry of the Siberian Trap of the Noril'sk area, USSR, with implications for the relative contributions of crust and mantle to flood basalt volcanism, *Contrib. Mineral. Petrol.*, *104*, 631–644.

Mahoney, J. J. (1988), Deccan Traps, in *Continental Flood Basalts*, edited by J. D. Macdougall, pp. 151–194, Springer, New York.

Mahoney, J. J., , and M. F. Coffin (Eds.) (1997), *Large Igneous Provinces: Continental, Oceanic and Planetary Flood Volcanism*, *Geophys. Monogr. Ser.*, vol. 100, 438 pp., AGU, Washington, D. C.

McDonough, W. F., and S.-S. Sun (1995), The composition of the Earth, *Chem. Geol.*, *120*, 223–253.

Milanovskiy, Y. Y. (1976), Rift zones of the geologic past and their associated formations, *Int. Geol. Rev.*, *18*, 619–639.

Molzahn, M., L. Reisberg, and G. Woerner (1996), Os, Sr, Nd, Pb, O isotope and trace element data from the Ferrar flood basalts, Antarctica: Evidence for an enriched subcontinental lithospheric source, *Earth Planet. Sci. Lett.*, *144*, 529–545.

Nelson, D. R. (1992), Isotopic characteristics of potassic rocks: Evidence for the involvement of subducted sediments in magma genesis, *Lithos*, *28*, 403–420.

Phipps Morgan, J., and J. W. Morgan (1998), Two-stage melting and the geochemical evolution of the mantle: A recipe for mantle plum-pudding, *Earth Planet. Sci. Lett.*, *170*, 215–239.

Reichow, M. K., A. D. Saunders, R. V. White, A. L. Al'Mukhamedov, and A. Y. Medvedev (2005), Geochemistry and petrogenesis of basalts from the West Siberian Basin: An extension of the Permo-Triassic Siberian Traps, *Lithos*, *79*, 425–452.

Reisberg, L., A. Zindler, F. Marcantonio, W. White, D. Wyman, and B. Weaver (1993), Os isotope systematics in ocean island basalts, *Earth Planet. Sci. Lett.*, *120*, 149–167.

Richards, M. A., R. A. Duncan, and V. E. Courtillot (1989), Flood basalts and hot-spot tracks: Plume heads and tails, *Science*, *246*, 103–107.

Ringwood, A. E., S. E. Kesson, W. Hibberson, and N. Ware (1992), Origin of kimberlites and related magmas, *Earth Planet. Sci. Lett.*, *113*, 521–538.

Roy-Barman, M., and C. J. Allègre (1994), $^{187}Os/^{188}Os$ ratios of mid-ocean ridge basalts and abyssal peridotites, *Geochim. Cosmochim. Acta*, *58*, 5043–5054.

Salters, V. J. M., and A. Stracke (2004), Composition of the depleted mantle, *Geochem. Geophys. Geosyst.*, *5*, Q05B07, doi:10.1029/2003GC000597.

Saunders, A. D., J. G. Fitton, A. C. Kerr, M. J. Norry, and R. W. Kent (1997), The North Atlantic Igneous Province, in *Large Igneous Provinces: Continental, Oceanic and Planetary Flood Volcanism*, *Geophys. Monogr. Ser.*, vol. 100, edited by J. J. Mahoney and M. F. Coffin, pp. 95–122, AGU, Washington, D. C.

Saunders, A. D., R. W. England, M. K. Reichow, and R. V. White (2005), A mantle plume origin for the Siberian traps: Uplift and extension in the West Siberian Basin, Russia, *Lithos*, *79*, 407–424.

Sharma, M., A. R. Basu, and G. V. Nesternko (1991), Nd-Sr isotopes, petrochemistry, and origin of the Siberian flood basalts, USSR, *Geochim. Cosmochim. Acta*, *55*, 1183–1192.

Sharma, M., A. R. Basu, and G. V. Nesterenko (1992), Temporal, Sr-, Nd-, and Pb-isotopic variations in the Siberian flood basalts: Implications for the plume source characteristics, *Earth Planet. Sci. Lett.*, *113*, 365–381.

Sobolev, A. V., V. S. Kamenetsky, and N. N. Kononkova (1992), New data on Siberian meymechite petrology, *Geochem. Int.*, *29*, 10–20.

Sun, S.-S., and W. F. McDonough (1989), Chemical and isotopic systematics of oceanic basalts: Implications for mantle composition and processes, in *Magmatism in the Ocean Basins*, edited by A. D. Saunders and M. J. Norry, *Geol. Soc. Spec. Publ.*, 42, 313–345.

Todt, W., R. A. Cliff, A. Hanser, and A. W. Hofmann (1996), Evaluation of a ^{202}Pb-^{205}Pb double spike for high-precision lead isotope analysis, in *Earth Processes: Reading the Isotope Code*, *Geophys. Monogr. Ser.*, vol. 95, edited by S. R. Hart and A. Basu, pp. 429–437, AGU, Washington, D. C.

Walker, R. J., J. W. Morgan, M. F. Horan, G. K. Czamanske, E. J. Krogstad, A. P. Likhachev, and V. E. Kunilov (1994), Re-Os isotopic evidence for an enriched mantle source for the Noril'sk-type ore-bearing intrusions, Siberia, *Geochim. Cosmochim. Acta*, *58*, 4179–4197.

Walker, R. J., J. W. Morgan, E. S. Beary, M. I. Smoliar, G. K. Czamanske, and M. F. Horan (1997), Applications of the ^{190}Pt-^{186}Os isotope system to geochemistry and cosmochemistry, *Geochim. Cosmochim. Acta*, *61*, 4799–4807.

Walker, R. J., H. M. Prichard, A. Ishiwatari, and M. Pimentel (2002), The osmium isotopic composition of the convecting upper mantle deduced from ophiolite chromitites, *Geochim. Cosmochim. Acta*, *66*, 329–345.

White, R., and D. McKenzie (1989), Magmatism at rift zones: The generation of volcanic continental margins and flood basalts, *J. Geophys. Res.*, *94*, 7685–7729.

Wooden, J. L., G. K. Czamanske, V. A. Fedorenko, N. T. Arndt, C. Chauvel, R. M. Bouse, B.-S. W. King, R. J. Knight, and D. F. Siems (1993), Isotopic and trace-element constraints on mantle and crustal contributions to Siberian continental flood basalts, Noril'sk area, Siberia, *Geochim. Cosmochim. Acta*, *57*, 3677–3704.

Wright, T. L., M. Mangan, and D. A. Swanson (1989), Chemical data for flows and feeder dikes of the Yakima basalt subgroup, Columbia River basalt group, Washington, Oregon, and Idaho, and their bearing on a petrogenetic model, *U.S. Geol. Surv. Bull.*, *1821*, 1–71.

Zindler, A., and S. Hart (1986), Chemical geodynamics, *Annu. Rev. Earth Planet. Sci.*, *14*, 493–571.